Azimuthal spin asymmetries in light-cone constituent quark models

S. Boffi,[1,2] A. V. Efremov,[3] B. Pasquini,[1,2] and P. Schweitzer[4]

[1]*Dipartimento di Fisica Nucleare e Teorica, Università degli Studi di Pavia, Pavia, Italy*
[2]*Istituto Nazionale di Fisica Nucleare, Sezione di Pavia, Pavia, Italy*
[3]*Joint Institute for Nuclear Research, Dubna, 141980 Russia*
[4]*Department of Physics, University of Connecticut, Storrs, Connecticut 06269, USA*

We present results for all leading-twist azimuthal spin asymmetries in semi-inclusive lepton-nucleon deep-inelastic scattering due to T-even transverse-momentum dependent parton distribution functions on the basis of a light-cone constituent quark model. Attention is paid to discuss the range of applicability of the model, especially with regard to the scale dependence of the observables and the transverse-momentum dependence of the distributions. We find good agreement with available experimental data and present predictions to be further tested by future CLAS, COMPASS, and HERMES data.

I. INTRODUCTION

The composite nature of the nucleon has been explored for a long time by means of deep-inelastic scattering (DIS) of a lepton beam in the Bjorken regime, i.e., when q and P denote the four-momentum transfer and the nucleon momentum, in the limit of $P \cdot q$ and $Q^2 = -q^2 \to \infty$, while $x = Q^2/(2P \cdot q)$ is fixed. As a consequence of the high scale Q, scattering occurs in a collinear configuration between the incident lepton and a single "parton" in the nucleon. The factorization theorem allows the inclusive DIS cross section to be expressed as a convolution of two contributions: one corresponds to the hard process occurring at short distance between probe and parton; the other accounts for the coherent long-distance interactions between parton and target, and is described in terms of parton distributions. At leading order (leading twist) x can be interpreted as the fraction of the longitudinal momentum of the parent (fast-moving) nucleon carried by the active parton, and one may distinguish three kinds of parton distributions. Two of them are well known from measurements of structure functions in DIS and other processes: $f_1^a(x)$ is the probability density of finding an unpolarized parton with longitudinal momentum fraction x in an unpolarized nucleon, and $g_1(x)$ gives the net helicity of partons in a longitudinally polarized nucleon. The third one, the (chiral-odd) transversity $h_1(x)$ describing the number density of partons with polarization parallel to that of a transversely polarized nucleon minus the number density of partons with antiparallel polarization, requires a quark helicity flip that cannot be achieved in the inclusive DIS. Other processes have to be explored for that.

However, in addition to the information on the longitudinal behavior in momentum space along the direction in which the nucleon is moving, a complete three-dimensional picture of the nucleon also requires knowledge of the transverse motion of partons [1,2]. A full account of the orbital motion, which is also an important issue to understand the spin structure of the nucleon, can be given in terms of transverse-momentum dependent parton distribution functions (TMDs). There are eight leading-twist TMDs $f_1(x, p_T)$, $f_{1T}^\perp(x, p_T)$, $g_{1L}(x, p_T)$, $g_{1T}(x, p_T)$, $h_1(x, p_T)$, $h_{1L}^\perp(x, p_T)$, $h_{1T}^\perp(x, p_T)$, $h_1^\perp(x, p_T)$ [3]. Two of them, the Boer-Mulders and Sivers functions $h_1^\perp(x, p_T)$ and $f_{1T}^\perp(x, p_T)$ [3,4], are T-odd, i.e., they change sign under naïve time reversal, which is defined as usual time reversal, but without interchange of initial and final states. The other six leading-twist TMDs are T-even.

In order to be sensitive to intrinsic transverse parton momenta it is necessary to measure adequate transverse momenta of the produced hadrons in the final state, e.g., in processes like semi-inclusive lepton-nucleon DIS (SIDIS), hadron production in $e^+ e^-$ annihilation or the Drell-Yan processes in hadron-hadron collisions [1–21].

Here, factorization has been proved at leading twist [22–25] allowing to access information on TMDs as well as on fragmentation functions (FFs) describing the hadronization process of the hit quark decaying into the detected hadrons. At leading twist, the fragmentation of unpolarized hadrons is described in terms of two fragmentation functions, $D_1(z, K_T)$ and $H_1^\perp(z, K_T)$, where z is the energy fraction taken out by the detected hadron and $K_T = |\boldsymbol{K}_T|$ its transverse momentum. The function $D_1(z, K_T)$ describes the decay of an unpolarized quark, whereas the Collins function $H_1^\perp(z, K_T)$ describes a left-right asymmetry in the decay of a transversely polarized quark [7–9].

By measuring the angular distribution of produced hadrons, in SIDIS it is possible to access information on all eight leading-twist TMDs in combinations with the two leading-twist FFs. Restricting ourselves to the one-photon-exchange approximation and considering spin degrees of freedom such as the beam helicity and the target spin, the contraction between the lepton and hadron tensors in the SIDIS lepton-nucleon cross section can be decomposed in a model-independent way in terms of 18 structure functions, thus exhibiting a nontrivial azimuthal dependence of the detected hadron around the (spacelike) direction de-

fined by the virtual photon [10,26–30]. According to factorization each of the leading-twist structure functions can be conceived as a convolution between one TMD and one FF. Since structure functions enter the cross section with a defined angular coefficient, they can be accessed by looking at specific azimuthal SIDIS asymmetries. This has become now a powerful tool for studying the three-dimensional structure of the nucleon [31–48], and many more data are expected to come in the future. The remarkable experimental progress was accompanied by and motivated numerous theoretical and phenomenological studies in the literature [49–87].

In this paper we compute azimuthal spin asymmetries due to the T-even transverse-momentum dependent parton distributions functions. For that we use the predictions from the light-cone constituent quark model (CQM) of Ref. [78], which has been successfully applied also in the calculation of electroweak properties of the nucleon [88] and generalized parton distributions [89]. Such a model, based on the light-cone wave function (LCWF) overlap representation of TMDs, is well suited to illustrate the relevance of the different orbital angular momentum components of the nucleon wave function for the respective observables. To best of our knowledge, this is the first attempt to describe all leading-twist spin asymmetries in SIDIS due to T-even TMDs in a single approach. We include also studies of the far better known collinear double-spin asymmetries A_1 and A_{LL}—not only for sake of completeness, but also to demonstrate the capability of the approach to describe reliably the gross features of spin effects in the nucleon.

The article is organized as follows: In Sec. II, the relevant definitions of azimuthal asymmetries in SIDIS are recalled. In Sec. III, the main ingredients of the light-cone CQM of Ref. [78] are reviewed, and the results for T-even TMDs discussed. In Sec. IV, we first study the collinear double-spin asymmetries A_1 and A_{LL}. This and the following Sec. V devoted to a discussion of the transverse-momentum dependence of the TMDs, help to assert the range of applicability of the approach. In Secs. VI, VII, VIII, and IX, we evaluate the leading-twist azimuthal double and single-spin asymmetries due to T-even TMDs—focusing on their x dependence. Section X exemplifies how the approach can be applied to make predictions for the transverse hadron momentum dependence of spin asymmetries. Concluding remarks are given in Sec. XI. Finally, a more detailed discussion about the model predictions for the sensitivity of the azimuthal asymmetries on different orbital angular momentum components are discussed in the Appendix.

II. SPIN AND AZIMUTHAL ASYMMETRIES IN SIDIS

The SIDIS process is sketched in Fig. 1. Let us denote the momenta of the target, incoming and outgoing lepton by P, l and l' and introduce the four-momentum transfer $q = l - l'$ with $Q^2 = -q^2$. Then the relevant SIDIS variables are defined as $x = Q^2/(2P \cdot q)$, $y = (P \cdot q)/(P \cdot l)$, and $z = (P \cdot P_h)/(P \cdot q)$. The component of the momentum of the produced hadron transverse with respect to the virtual photon is denoted by $\boldsymbol{P}_{h\perp}$ and $P_{h\perp} = |\boldsymbol{P}_{h\perp}|$.

The SIDIS cross section (differential in x, y, z and the azimuthal angle ϕ_h of the produced hadron defined in Fig. 1) has the following general decomposition [10,27], where σ_0 is the spin- and ϕ-independent part of the cross section, and where the dots indicate power suppressed ("-subleading-twist") terms,

$$\frac{d^4\sigma}{dxdydzd\phi_h} = \frac{d^4\sigma_0}{dxdydzd\phi_h}\{1 + \cos(2\phi_h)p_1(y)A_{UU}^{\cos(2\phi_h)} + S_L\sin(2\phi_h)p_1(y)A_{UL}^{\sin(2\phi_h)} + \lambda S_L p_2(y)A_{LL}$$

$$+ \lambda S_T\cos(\phi_h - \phi_S)p_2(y)A_{LT}^{\cos(\phi_h - \phi_S)} + S_T\sin(\phi_h - \phi_S)A_{UT}^{\sin(\phi_h - \phi_S)} + S_T\sin(\phi_h + \phi_S)p_1(y)A_{UT}^{\sin(\phi_h + \phi_S)}$$

$$+ S_T\sin(3\phi_h - \phi_S)p_1(y)A_{UT}^{\sin(3\phi_h - \phi_S)}\} + \ldots \tag{1}$$

with

$$p_1(y) = \frac{1 - y}{1 - y + \frac{1}{2}y^2}, \qquad p_2(y) = \frac{y(1 - \frac{1}{2}y)}{1 - y + \frac{1}{2}y^2}. \tag{2}$$

In A_{XY}^{weight} the index X describes the beam polarization, which is unpolarized (U) or longitudinal (L, characterized then by the beam helicity λ). The index Y denotes the target polarization, which is unpolarized (U), longitudinal (L) or transverse (T) with respect to the virtual photon. In experiments the target is polarized with respect to the beam, of course, but this is up to corrections of $\mathcal{O}(1/Q)$ the same. As we shall deal with leading-twist observables,
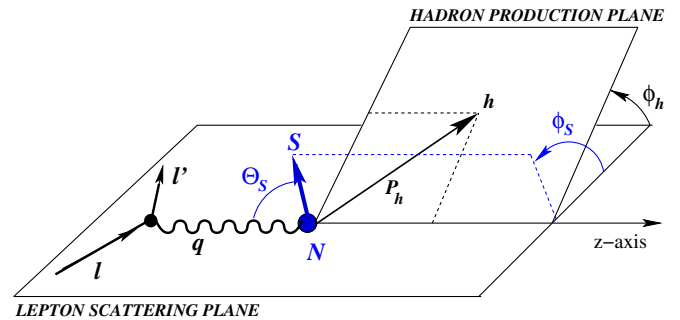
FIG. 1 (color online). Kinematics of the SIDIS process $lN \to l'hX$ and the definitions of azimuthal angles in the lab frame.

such corrections will be neglected throughout. The superscript "weight" reminds us of the kind of angular distribution of the produced hadrons with no index indicating an isotropic ϕ distribution, and ϕ_S is the azimuthal angle of the target's transverse polarization vector, see Fig. 1. The asymmetries are defined in terms of structure functions $A_{XY}^{\text{weight}} = F_{XY}^{\text{weight}}/F_{UU}$, and the latter have the following partonic (tree-level) description in the Bjorken-limit [3,11]

$$F_{UU} = \mathcal{C}[f_1 D_1], \tag{3}$$

$$F_{LL} = \mathcal{C}[g_{1L} D_1], \tag{4}$$

$$F_{UT}^{\sin(\phi_h - \phi_S)} = -\mathcal{C}\left[\frac{\boldsymbol{h}_\perp \cdot \boldsymbol{p}_T}{M} f_{1T}^\perp D_1\right], \tag{5}$$

$$F_{LT}^{\cos(\phi_h - \phi_S)} = \mathcal{C}\left[\frac{\boldsymbol{h}_\perp \cdot \boldsymbol{p}_T}{M} g_{1T} D_1\right], \tag{6}$$

$$F_{UT}^{\sin(\phi_h + \phi_S)} = \mathcal{C}\left[\frac{\boldsymbol{h}_\perp \cdot \boldsymbol{K}_T}{z m_h} h_1 H_1^\perp\right], \tag{7}$$

$$F_{UU}^{\cos(2\phi_h)} = \mathcal{C}\left[\frac{2(\boldsymbol{h}_\perp \cdot \boldsymbol{K}_T)(\boldsymbol{h}_\perp \cdot \boldsymbol{p}_T) - \boldsymbol{K}_T \cdot \boldsymbol{p}_T}{z m_h M} h_1^\perp H_1^\perp\right], \tag{8}$$

$$F_{UL}^{\sin(2\phi_h)} = \mathcal{C}\left[\frac{2(\boldsymbol{h}_\perp \cdot \boldsymbol{K}_T)(\boldsymbol{h}_\perp \cdot \boldsymbol{p}_T) - \boldsymbol{K}_T \cdot \boldsymbol{p}_T}{z m_h M} h_{1L}^\perp H_1^\perp\right], \tag{9}$$

$$F_{UT}^{\sin(3\phi_h - \phi_S)} = -\mathcal{C}\left[\frac{2(\boldsymbol{h}_\perp \cdot \boldsymbol{p}_T)(\boldsymbol{p}_T \cdot \boldsymbol{K}_T) + \boldsymbol{p}_T^2(\boldsymbol{h}_\perp \cdot \boldsymbol{K}_T) - 4(\boldsymbol{h}_\perp \cdot \boldsymbol{p}_T)^2(\boldsymbol{h}_\perp \cdot \boldsymbol{K}_T)}{2 z m_h M^2} h_{1T}^\perp H_1^\perp\right], \tag{10}$$

where $\boldsymbol{h}_\perp = \boldsymbol{P}_{h\perp}/P_{h\perp}$ and M (m_h) is the mass of the nucleon (produced hadron). The convolution is defined as

$$\mathcal{C}[w j J] = \int d^2 \boldsymbol{p}_T \int d^2 \boldsymbol{K}_T \delta^{(2)}(z\boldsymbol{p}_T + \boldsymbol{K}_T - \boldsymbol{P}_{h\perp}) w(\boldsymbol{p}_T, \boldsymbol{K}_T)$$
$$\times \sum_a e_a^2 x j^a(x, p_T) J^a(z, K_T), \tag{11}$$

where $p_T = |\boldsymbol{p}_T|$. These convolution integrals can be solved analytically only in the case of the structure functions F_{UU} and F_{LL}, in which case the weight function w in Eq. (11) is simply unity. The unpolarized cross section is given in terms of F_{UU} by

$$\frac{d^4\sigma_0}{dx dy dz d\phi_h} = \frac{2\alpha^2 s}{Q^4}\left(1 - y + \frac{y^2}{2}\right) F_{UU}(x, z),$$
$$F_{UU}(x, z) = \sum_a e_a^2 x f_1^a(x) D_1^a(z). \tag{12}$$

Recalling the notation $g_1^a(x) = \int d^2 \boldsymbol{p}_T g_{1L}^a(x, p_T)$, the double-spin asymmetry A_{LL} is given as follows:

$$A_{LL} = \frac{F_{LL}}{F_{UU}} = \frac{\sum_a e_a^2 x g_1^a(x) D_1^a(z)}{\sum_a e_a^2 x f_1^a(x) D_1^a(z)}. \tag{13}$$

If no hadron is observed in the final state, the inclusive version of the double-spin asymmetry (13) is commonly referred to as A_1 and given by

$$A_1 = \frac{\sum_a e_a^2 x g_1^a(x)}{\sum_a e_a^2 x f_1^a(x)}. \tag{14}$$

For all other structure functions (5)–(10) the convolution integrals cannot be solved analytically, unless one assumes models for the transverse parton momentum dependence of TMDs. A popular model is the Gaussian Ansatz, where one assumes

$$j^a(x, p_T) = j^a(x) \frac{\exp(-p_T^2/\langle p_T^2(j)\rangle)}{\pi\langle p_T^2(j)\rangle},$$
$$J^a(z, K_T) = J^a(z) \frac{\exp(-K_T^2/\langle K_T^2(J)\rangle)}{\pi\langle K_T^2(J)\rangle} \tag{15}$$

for some generic transverse parton momentum dependent distribution $j^a(x, p_T)$ and fragmentation $J^a(z, K_T)$ functions. This is, of course, a crude approximation. However, besides being convenient [11], this Ansatz is also phenomenologically useful, provided the transverse hadron momenta are small compared to the relevant hard scale, $\langle P_{h\perp}\rangle \ll Q$ in SIDIS, and one is interested in catching the gross features of the effects [53]. A high precision description of p_T effects requires methods along the QCD-based formalism of [6], see [90] and references therein for examples.

Using this Ansatz we obtain the following results:

$$F_{UT}^{\sin(\phi_h - \phi_S)} = -B_0 \sum_a e_a^2 x f_{1T}^{\perp(1)a}(x) D_1^a(z),$$
$$B_0 = \frac{\sqrt{\pi} M}{\{\langle p_T^2(f_{1T}^\perp)\rangle + \langle K_T^2(D_1)\rangle/z^2\}^{1/2}}, \tag{16}$$

$$F_{LT}^{\cos(\phi_h - \phi_S)} = B_0' \sum_a e_a^2 x g_{1T}^{(1)a}(x) D_1^a(z),$$
$$B_0' = \frac{\sqrt{\pi} M}{\{\langle p_T^2(g_{1T})\rangle + \langle K_T^2(D_1)\rangle/z^2\}^{1/2}}, \tag{17}$$

$$F_{UT}^{\sin(\phi_h + \phi_S)} = B_1 \sum_a e_a^2 x h_1^a(x) H_1^{\perp(1/2)a}(z),$$
$$B_1 = \frac{2}{\{1 + R(h_1)\}^{1/2}}, \tag{18}$$

$$F_{UU}^{\cos(2\phi_h)} = B_2 \sum_a e_a^2 x h_1^{\perp(1)a}(x) H_1^{\perp(1/2)a}(z),$$

$$B_2 = \frac{8zM[\pi\langle K_T^2(H_1^\perp)\rangle]^{-1/2}}{1 + R(h_1^\perp)},$$

(19)

$$F_{UL}^{\sin(2\phi_h)} = B_2' \sum_a e_a^2 x h_{1L}^{\perp(1)a}(x) H_1^{\perp(1/2)a}(z),$$

$$B_2' = \frac{8zM[\pi\langle K_T^2(H_1^\perp)\rangle]^{-1/2}}{1 + R(h_{1L}^\perp)},$$

(20)

$$F_{UT}^{\sin(3\phi_h - \phi_S)} = -B_3 \sum_a e_a^2 x h_{1T}^{\perp(1)a}(x) H_1^{\perp(1/2)a}(z),$$

$$B_3 = \frac{3}{\{R(h_{1T}^\perp)^{1/3} + R(h_{1T}^\perp)^{-1/3}\}^{3/2}},$$

(21)

where

$$j^a(x) = \int d^2\boldsymbol{p}_T j^a(x, p_T),$$

$$j^{(1)a}(x) = \int d^2\boldsymbol{p}_T \frac{p_T^2}{2M^2} j^a(x, p_T),$$

(22)

$$H_1^{\perp(1/2)a}(z) = \int d^2\boldsymbol{K}_T \frac{K_T}{2zm_h} H_1^{\perp a}(z, K_T),$$

$$R(j) = \frac{z^2\langle p_T^2(j)\rangle}{\langle K_T^2(H_1)\rangle}.$$

(23)

Of course, other models of p_T dependence can also be assumed. In that case, however, one typically cannot solve the convolution analytically, as in Eqs. (16)–(21), and has to use numerical integration.

Notice that one could avoid the model dependence at this point by including adequate powers of transverse hadron momentum in the weights of the asymmetries [3]. The analysis of such $P_{h\perp}$-weighted asymmetries is more involved, and so far only preliminary data not corrected for acceptance effects have been shown [39].

III. TMDS IN THE LIGHT-CONE CONSTITUENT QUARK MODEL

A convenient way to describe parton distributions is to use the representation in terms of overlaps of LCWFs. This representation can be viewed as a generalization of the famous Drell-Yan formula for electromagnetic form factors [91], and it was recently derived and applied in phenomenological calculations for the generalized parton distributions [92,93] and transverse-momentum dependent parton distributions [78,94]. In practice, this representation becomes useful in phenomenological applications where one can reasonably truncate the expansion of the hadron state to the Fock components with a few partons. In our approach, we consider the minimum Fock sector with just three valence quarks. This truncation allows to describe the

parton distributions in those kinematical regions where the valence degrees of freedom are effective, while the contributions from quarks and gluons are suppressed.

The three-quark component of the nucleon has been studied extensively in the literature [95–101] in terms of quark distribution amplitudes defined as hadron-to-vacuum transition matrix elements of nonlocal gauge-invariant light-cone operators. Unlike these works, the authors of Refs. [94,102,103] considered the wave-function amplitudes keeping full transverse-momentum dependence of partons and proposed a systematic way to enumerate independent amplitudes of a LCWF given a particular parton combination. Within this general classification scheme, one finds that the nucleon state with three valence quarks has six independent scalar amplitudes, which serve to parametrize the contribution from the four different orbital angular momentum components L_z compatible with total angular momentum conservation, i.e., $L_z = 0, \pm 1, 2$. An application of this method has been developed in Ref. [78] for the calculation of the TMDs within a light-cone CQM, which will be used here to make quantitative estimates of the azimuthal asymmetries. The key ingredient of the model is to derive the LCWF by boosting equal-time model wave function. The equal-time wave function is constructed as a product of a momentum wave function, which is in a pure S-wave state and invariant under permutations, and a spin-isospin wave function, which is uniquely determined by SU(6) symmetry requirements. The corresponding solution in light-cone dynamics is obtained through the unitary Melosh rotations acting on the spin of the individual quarks. By applying the Melosh rotations, the Pauli spinors of the quarks in the nucleon rest frame are converted into light-cone spinors. The effects of the relativistic spin dynamics are evident in the presence of spin-flip terms in the Melosh rotations generating nonzero orbital angular momentum components, which can be mapped out into six independent scalar amplitudes. The explicit expressions of these light-cone amplitudes can be found in Ref. [78], while the corresponding results for the TMDs are given by

$$f_1^a(x, p_T) = N^a \int d[X]\delta(x - x_3)\delta(\boldsymbol{p}_T - \boldsymbol{p}_{\perp 3})$$
$$\times |\psi(\{x_i\}, \{\boldsymbol{p}_{\perp i}\})|^2,$$

(24)

$$g_{1L}^a(x, p_T) = P^a \int d[X]\delta(x - x_3)\delta(\boldsymbol{p}_T - \boldsymbol{p}_{\perp 3})$$
$$\times \frac{(m + xM_0)^2 - \boldsymbol{p}_T^2}{(m + xM_0)^2 + \boldsymbol{p}_T^2} |\psi(\{x_i\}, \{\boldsymbol{p}_{\perp i}\})|^2,$$

(25)

$$g_{1T}^a(x, p_T) = P^a \int d[X]\delta(x - x_3)\delta(\boldsymbol{p}_T - \boldsymbol{p}_{\perp 3})$$
$$\times \frac{2M(m + xM_0)}{(m + xM_0)^2 + \boldsymbol{p}_T^2} |\psi(\{x_i\}, \{\boldsymbol{p}_{\perp i}\})|^2,$$

(26)

$$h_1^a(x, p_T) = P^a \int d[X]\delta(x - x_3)\delta(\boldsymbol{p}_T - \boldsymbol{p}_{\perp 3})$$

$$\times \frac{(m + xM_0)^2}{(m + xM_0)^2 + \boldsymbol{p}_T^2}|\psi(\{x_i\}, \{\boldsymbol{p}_{\perp i}\})|^2, \quad (27)$$

$$h_{1T}^{\perp a}(x, p_T) = -P^a \int d[X]\delta(x - x_3)\delta(\boldsymbol{p}_T - \boldsymbol{p}_{\perp 3})$$

$$\times \frac{2M^2}{(m + xM_0)^2 + \boldsymbol{p}_T^2}|\psi(\{x_i\}, \{\boldsymbol{p}_{\perp i}\})|^2,$$

$$(28)$$

$$h_{1L}^{\perp a}(x, p_T) = -P^a \int d[X]\delta(x - x_3)\delta(\boldsymbol{p}_T - \boldsymbol{p}_{\perp 3})$$

$$\times \frac{2M(m + xM_0)}{(m + xM_0)^2 + \boldsymbol{p}_T^2}|\psi(\{x_i\}, \{\boldsymbol{p}_{\perp i}\})|^2,$$

$$(29)$$

where we introduced the integration measure

$$d[X] = dx_1 dx_2 dx_3 \delta\left(1 - \sum_{i=1}^{3} x_i\right)$$

$$\times \frac{d^2\boldsymbol{p}_{\perp 1}d^2\boldsymbol{p}_{\perp 2}d^2\boldsymbol{p}_{\perp 3}}{[2(2\pi^3)]^2}\delta\left(\sum_{i=1}^{3}\boldsymbol{p}_{\perp i}\right). \quad (30)$$

In Eqs. (24)–(29), M_0 is the mass of the noninteracting three-quark system, and m the constituent quark mass. Furthermore, the flavor dependence is given by the factors $N^u = 2$, $N^d = 1$, and $P^u = 4/3$, $P^d = -1/3$, as dictated by SU(6) symmetry. A further consequence of the assumed SU(6) symmetry is the factorization in Eqs. (24)–(29) of the momentum-dependent wave function $\psi(\{x_i\}, \{\boldsymbol{p}_{\perp i}\})$ from the spin-dependent factor arising from the Melosh rotations. Thanks to this factorized form one finds the following relations:

$$2h_1^a(x, p_T) = g_{1L}^a(x, p_T) + \frac{P^a}{N^a}f_1^a(x, p_T), \quad (31)$$

$$\frac{P^a}{N^a}f_1^a(x, p_T) = h_1^a(x, p_T) - \frac{p_T^2}{2M^2}h_{1T}^{\perp a}(x, p_T), \quad (32)$$

$$h_{1L}^{\perp q}(x, p_T) = -g_{1T}^a(x, p_T). \quad (33)$$

Equation (31) is a generalization of the analogous relations discussed in [56,104] and was also rederived together with Eq. (32) in Ref. [77]. Equation (33) was already found in the diquark spectator model of Ref. [76]. In QCD the various TMDs are all independent of each other, and describe different aspects of the nucleon structure. However, it is natural to encounter relations among TMDs in simple models limiting the valence-quark contribution and imposing SU(6) symmetry. The specific form of the relations can be traced back to the Melosh rotations, which relate longitudinal and transverse nucleon polarization states in a Lorentz-invariant way. A similar situation

occurs with the bag model [77]. In the diquark spectator model of Ref. [76] the relations (31) and (32) hold only for the separate scalar and axial contributions, while Eq. (33) is verified more generally for both u and d flavors. Since only two out of the four functions f_1, g_{1L}, h_1, $h_{1T}^{\perp}$ are linearly independent, there are numerous relations among them. For example, subtracting (31) and (32) one gets a particularly interesting relation between pretzelosity, transversity, and helicity distribution [77]

$$g_1^a(x, p_T) - h_1^a(x, p_T) = h_{1T}^{\perp(1)a}(x, p_T). \quad (34)$$

This relation was recently discussed also in connection with the quark orbital angular momentum distribution [80]. In the version of the diquark spectator model of Ref. [79] the relation (34) is not supported in the axial-vector diquark sector, but it remains valid for the scalar sector (see also [80,81]). Interestingly, in Ref. [82] the $h_{1T}^{\perp}(x, p_T)$ distribution was reconsidered also within a covariant parton model with the remarkable finding that the model satisfies the relation (34) without assuming SU(6) symmetry.

The results in Eqs. (24)–(29) are applied in the following to a specific CQM taking the form of the momentum wave function from Ref. [105]

$$\psi(\{x_i, \boldsymbol{p}_{\perp i}\}) = 2(2\pi)^3\left[\frac{1}{M_0}\frac{\omega_1\omega_2\omega_3}{x_1x_2x_3}\right]^{1/2}\frac{N'}{(M_0^2 + \beta^2)^\gamma}, \quad (35)$$

where ω_i is the free-quark energy and N' is a normalization factor such that $\int d[X]|\psi(\{x_i\}, \{\boldsymbol{p}_{\perp i}\})|^2 = 1$. In Eq. (35), the scale β, the parameter γ for the power-law behavior, and the quark mass m are taken from Ref. [105], i.e., $\beta = 0.607$ GeV, $\gamma = 3.4$, and $m = 0.267$ GeV. According to the analysis of Ref. [106] these values lead to a very good description of many baryonic properties.

The results Eqs. (24)–(29) are general and can be applied to any CQM adopting the appropriate nucleon wave function. For example, we also considered the prediction in the hypercentral CQM model of Refs. [107,108]. It has been observed that the description of nucleon properties using the model wave function either from [106] or from [107,108] agree typically within (10–20)%, which might be considered as an indication of the accuracy of the CQM approach. In the following we shall assume that such is also the accuracy of the T-even TMDs from CQM [106]. The numerical results for T-even TMDs obtained in this way were discussed in detail in Ref. [78]. In order to compute T-odd TMDs it is necessary to go beyond the mere CQM scenario, and introduce gauge-boson degrees of freedom, which was beyond the scope of Ref. [78] and this work, where we concentrate on asymmetries due to T-even TMDs.

In Fig. 2, we show the results for the integrals in $\boldsymbol{p}_T$ of the TMDs defined in Eq. (22), omitting the flavor dependence given by the SU(6) isospin factors N^a and P^a in
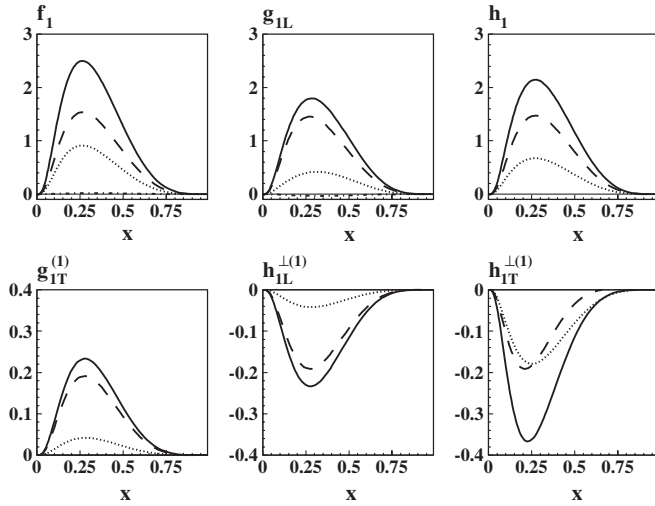
FIG. 2. Parton distribution functions and transverse moments of TMDs as functions of x from the light-cone CQM [78]. In all panels the solid curves show the total results for the "flavorless" TMDs, i.e., the TMDs of definite flavor follow from multiplying by the spin-flavor factors N^a or P^a, see Eqs. (24)–(29). The other curves show how much the different angular momentum components of the nucleon wave function contribute to the total results: In the case of $f_1(x)$, $g_1(x)$, $h_1(x)$, the dashed and dotted curves correspond to the contribution from the squares of the S- and P-wave components of the nucleon wave function, respectively. The D-wave contribution is absent in h_1, while for f_1 and g_1 it is quite small and corresponds to the hardly visible dashed-dotted curves. In the case of $g_{1T}^{(1)}(x)$, $h_{1L}^{(1)\perp}(x)$ the dashed and dotted curves give the results from the S-P and P-D interference terms, respectively. In the case of $h_{1T}^{(1)\perp}(x)$, the dashed curve is the result from the P-wave interference, and the dotted curve is due to the interference of S and D waves.

Eqs. (29). The solid curves correspond to the total results, obtained as the sum of the partial-wave contributions. The other curves show the contributions of the different orbital angular momentum components of the nucleon wave function. The unpolarized distribution f_1, the helicity distribution g_1, and the transversity h_1 involve matrix elements, which are all diagonal in the orbital angular momentum. In the plots of these functions, the dashed curves give the contribution from the S-wave component, and the dotted curves correspond to the P-wave contribution. The D wave gives a negligible contribution to the f_1 and g_1 distributions (dashed-dotted curves), while it is absent in the case of h_1. Although all these three functions are dominated by the S waves, they have a non-negligible contribution also from the P waves, with the largest (smallest) weight in the case of f_1 (g_1). The functions $g_{1T}^{(1)}$ and $h_{1L}^{(1)\perp}$ involve a transfer of orbital angular momentum by one unit between the initial and final nucleon state. In our model, they are simply related by Eq. (33). For these functions, the dashed curves in Fig. 2 show the contribution from the interference of S and P waves, and the dotted curves correspond to the results from the P- and D-wave interference term. The S-P

interference term gives the largest contribution in the full x range, while the P- and D-wave interference term contributes at most by 20%. In the case of $h_{1T}^{\perp(1)}$ one has a mismatch of orbital angular momentum between the initial and final nucleon state equal to $\Delta L_z = 2$. In the plot of this function in Fig. 2, the dashed curve gives the result for the interference of the $L_z = 1$ and $L_z = -1$ components, and the dotted curve refers to the contribution from the interference of the S- and D-wave components. Thanks to the interference with the S wave, we note that here the contribution from the D wave is amplified. Furthermore, at variance with the other distribution functions, the different partial-wave contributions do not have the same x dependence, and for $x \gtrsim 0.6$ the P waves are suppressed with respect to the S-D wave interference term. This peculiar behavior makes the $h_{1T}^{\perp(1)}$ function interesting, especially in the study of the interplay between the different partial-wave components in the azimuthal spin asymmetries, as discussed in the Appendix.

IV. COLLINEAR DOUBLE-SPIN ASYMMETRIES A_1 AND A_{LL}

Before discussing azimuthal asymmetries in SIDIS, we consider first the double-spin asymmetry A_{LL} and its inclusive analog A_1, Eqs. (13) and (14). The study of these observables in the model framework is instructive, because in this case evolution equations (and fragmentation functions) are known and complications due to p_T dependence are avoided. This allows us to test the model under "controlled conditions" in two respects. First, in which x range and with what accuracy is the model applicable? Of course, the performance of the model could vary with observables. Nevertheless, this exercise will give us valuable insights in this respect. Second, how stable are the results under evolution? In this case we can compare exact results, with results obtained making *assumptions* on the evolution. The experience made here will be useful later, when dealing with azimuthal asymmetries whose evolution is practically not solved.

A related key question emerging not only here but in any nonperturbative calculation concerns the scale at which the model results for the parton distributions hold. From the point of view of QCD where both quark and gluon degrees of freedom contribute, the role of the low-energy quark models is to provide initial conditions for the QCD evolution equations. Therefore, we assume the existence of a low scale Q_0^2 where glue and sea quark contributions are suppressed, and the dynamics inside the nucleon is described in terms of three valence (constituent) quarks confined by an effective long-range interaction. In fact, glue and sea quark degrees of freedom might be thought of at this low scale to be contained in the structure of the constituent quarks, which are massive objects. The actual value of Q_0^2 is fixed evolving back unpolarized data, until the valence distribution matches the condition that the

second moment, i.e., the momentum fraction carried by the valence quarks, is equal to one [109].

Using LO evolution equations, we find $Q_0^2 = 0.079$ GeV^2 [110]. Although there is no rigorous relation between the QCD quarks and the constituent quarks, and a more fundamental description of the transition from soft to hard regimes would be very helpful, this strategy reflects the present state of the art for quark model calculations [111–113], and has been validated with a fair comparison to experiments [109,111].

Figure 3(a) shows the inclusive double-spin asymmetry A_1 in DIS off proton, Eq. (14). The two theoretical curves are obtained using $g_1^a(x)$ and $f_1^a(x)$ from the light-cone CQM [78]. In one case both distribution functions are LO evolved from the low scale of the model Q_0^2 to $Q^2 = 3.0$ GeV^2 (solid curve) using the evolution codes of Refs. [114,115], and in the other case both distribution functions are taken at the low scale of the model (dashed curve). The results differ moderately at $x \gtrsim 0.1$ reflecting the weak scale dependence of A_1 [116].

As can be seen in Fig. 3(a), the description of data from the E143, EMC, and SMC experiments [117–119] is reasonable. For $x \gtrsim 0.15$ the model describes the A_1 data within an accuracy of about 30%. The description improves in the valence-x region of $x \gtrsim 0.2$ though the accuracy of the data at large x is not sufficient to draw definite conclusions. Since the model contains no antiquark and gluon degrees of freedom, it is not surprising to observe that it does not work at small x. As an intermediate summary, it can be said that the results are weakly scale dependent, and the model well catches the main features of the observable A_1 in its range of applicability, namely, in the valence-x region.

Since in the following we will deal with SIDIS, we repeat the exercise with the double-spin asymmetry A_{LL}, Eq. (13). Figures 3(b) and 3(c), show A_{LL} in DIS production of charged hadrons off proton target. The theoretical curves are obtained using $g_1^a(x)$ and $f_1^a(x)$ from the light-cone CQM [78], once LO evolved to $Q^2 = 2.5$ GeV^2

(solid curve), and once left at the initial scale of the model (dashed curve). For the fragmentation function $D_1^a(z)$ we use in both cases, and throughout this work, the LO parametrization [120] at $Q^2 = 2.5$ GeV^2. Again, we observe a weak scale dependence, and a good description of data in the valence x region, where the model describes the data within an accuracy of $\mathcal{O}(20\%)$. Thus, in the SIDIS case we make a comparably positive experience as in the inclusive case. Notice that the result with $g_1^a(x)$ and $f_1^a(x)$ taken at the low scale is, strictly speaking, not the consistent result for A_{LL} at such a low scale because we use the parametrization for D_1^a at $Q^2 = 2.5$ GeV^2.

We remark that we could have tried to describe the double-spin asymmetries A_1 and A_{LL} with $g_1^a(x)$ from the model, and $f_1^a(x)$ from a parametrization, for example [121]. Such an approach would correspond to the strategy to use the model only as input for the part which is responsible for the spin effect, and to use for the well-known denominator of the spin asymmetry standard parametrizations, which has the advantage that the model uncertainty is only in the numerator. In the case of A_1 and A_{LL}, however, such an approach yields a bad description of the data. This can be traced back to the fact that the $f_1^a(x)$ from the model [78] and from parametrizations [121] have different large-x behavior. Interestingly, it happens to be the case also in the case of $g_1^a(x)$ from the model [78] and from parametrizations [122], such that the uncertainties partly *cancel* in the ratio, leading to a better description of the data. It is important to stress that here we deal with chiral-even functions, where antiquark and gluon degrees of freedom are of importance. In the case of chiral-odd TMDs the situation is different, and a different approach could be more successful. We will come back to this point later on.

The above discussion allows to assign a "typical accuracy" to the approach. In this context it is of interest to make the following observation. The present version of the model uses SU(6) symmetry, such that $g_1^u(x) = -4g_1^d(x)$ at the low scale, and similarly for other polarized distribution
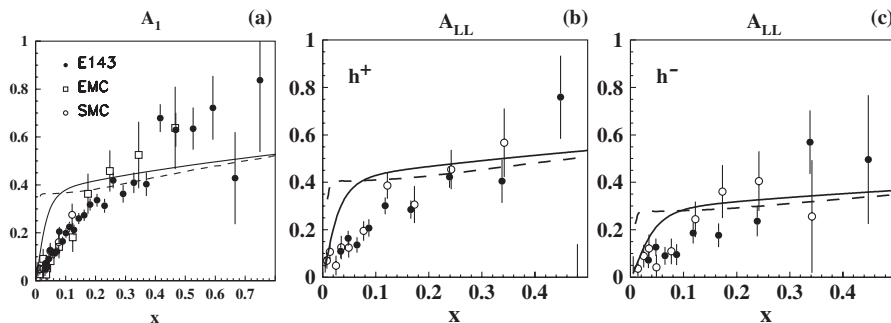
FIG. 3. The inclusive (a) and semi-inclusive (b, c) double-spin asymmetries, A_1 and A_{LL}, defined in Eqs. (13) and (14), in DIS off proton as functions of x. The theoretical curves are obtained with $g_1^a(x)$ and $f_1^a(x)$ from the light-cone CQM [78] as follows: both functions LO evolved to the $\langle Q^2 \rangle$ of the experiments (solid curves), and both at the low scale of the model (dashed curves). In (b, c) we use always the parametrization [120] for D_1^a at $Q^2 = 2.5$ GeV^2. The data in (a) are from Refs. [117–119], in (b,c) are from SMC (open circles) [142] and HERMES (solid circles) [143].

functions or TMDs. Because of isospin symmetry the structure functions of the neutron are related to those of the proton by interchanging u and d flavor. Therefore, at the low scale $A_1^n \propto \frac{4}{9} g_1^{u/n} + \frac{1}{9} g_1^{d/n} = \frac{4}{9} g_1^d + \frac{1}{9} g_1^u = 0$. At higher scales $A_1^n \neq 0$ due to evolution but the effect remains small. Rather than claiming $A_1^n \approx 0$, it is more meaningful to state that SU(6) predicts A_1^n to be small compared to, say, the A_1 of proton. Thus, for the SU(6) symmetry concept to be a useful tool, we expect for the ratio

$$\left| \frac{A_1^n}{A_1^p} \right| \ll 1. \tag{36}$$

Experimentally, A_1^n (extracted by subtracting deuteron and proton data, or from ^{3}He data, modulo nuclear corrections) is found clearly nonzero. However, in the valence-x region the SU(6) expectation is supported by data [123–128]: the ratio (36) is of the order of magnitude 20%—which is indeed a ''zero'' within the model accuracy.

Notice that in SIDIS the SU(6) symmetric TMDs are weighted with fragmentation functions, such that in general azimuthal asymmetries from the neutron are nonzero already at the low scale (with the exception of π^0 into which u and d quarks fragment with equal strength). Nevertheless, also in SIDIS the results for a neutron target are highly sensitive to SU(6) breaking effects, and we refrain from showing them here. An adequate description of spin asymmetries from a neutron target requires to account systematically for possible SU(6)-breaking effects. This is similar to what one observes in the case of the electric form factor of the neutron, where mixed-symmetry components in the nucleon wave function were found essential to reproduce the experimental data [88,129]. Results for the TMDs with such SU(6) breaking terms will be discussed elsewhere.

Let us draw conclusions from the study presented in this section. The double-spin asymmetries in inclusive DIS, A_1, and SIDIS, A_{LL}, are weakly scale dependent. The model describes the data on these observables within an accuracy of $\sim$20–30% in the valence-x region. This suggests that the approach could also be useful for studies of azimuthal spin asymmetries. In fact, at this point it is worth to stress that (i) azimuthal phenomena are expected to yield sizable effects especially in the valence-x region, (ii) *first* data on azimuthal asymmetries often have uncertainties comparable to the observed model accuracy, (iii) in proposals for future experiments predictions of new effects of an accuracy of $\mathcal{O}(30\%)$ are useful enough.

V. P_T DEPENDENCE, GAUSS ANSATZ, APPLICABILITY OF THE MODEL

When dealing with azimuthal asymmetries in SIDIS it is very convenient to use the Gaussian model for the distribution of transverse parton momenta, see Sec. II. If one

assumes the Gaussian Ansatz (15) for $f_1^a(x, p_T)$ and $D_1^a(z, K_T)$, then a good description of the SIDIS data (more precisely, *mean values* for $\langle P_{h\perp}(z) \rangle$ not corrected for acceptance effects) from HERMES [34] is obtained with the following parameters [59]:

$$\langle p_T^2(f_1) \rangle = 0.33 \text{ GeV}^2, \qquad \langle K_T^2(D_1) \rangle = 0.16 \text{ GeV}^2. \tag{37}$$

Numerically, very similar results were obtained in [57] from a study of EMC data [31] on the Cahn effect [5].

The p_T dependence of TMDs in the model [78] is definitely not of Gaussian form. (In fact, neither in this model, nor in any other model of TMDs considered so far [75–87], there is even the factorization of x and p_T dependence.) However, the essential question is: Can the p_T dependence be reasonably *approximated* by a Gaussian form?

In order to discuss that let us make the following two exercises: First, we define the mean transverse momenta ($n = 1$) and the mean square transverse momenta ($n = 2$) in the TMD $j(x, p_T)$ as follows:

$$\langle p_{T,j}^n \rangle = \frac{\int dx \int d^2 p_T \, p_T^n j(x, p_T)}{\int dx \int d^2 p_T \, j(x, p_T)}. \tag{38}$$

In Table I we show results for these quantities for T-even twist-2 TMDs from [78].

In order to see to which extent the results for the p_T dependence of TMDs from [78] can be approximated by a Gaussian behavior, we remind that in the Gaussian model the following relation holds:

$$\langle p_T^2 \rangle \overset{\text{Gauss}}{=} \frac{4}{\pi} \langle p_T \rangle^2. \tag{39}$$

In Table I we show also the results for the ratio $\frac{4\langle p_T \rangle^2}{\pi \langle p_T^2 \rangle}$ that would be unity for a Gaussian p_T distribution. Remarkably, the model results for this ratio from [78] deviate from unity by not more than 10%. Of course, although the Gaussian model relation (39) works within 10%, it does not necessarily imply that the p_T-dependence in the model is

TABLE I. The mean transverse momenta and the mean square transverse momenta of T-even TMDs, as defined in Eq. (38), from the light-cone CQM [78]. If the transverse momenta in the TMDs were Gaussian, then the result for the ratio in the fourth column would be unity, see text. The last column shows the $\langle p_T^2(j) \rangle$ in units of $\langle p_T^2(f_1) \rangle$.

TMD j	$\langle p_T \rangle$ in GeV	$\langle p_T^2 \rangle$ in GeV^2	$\frac{4\langle p_T \rangle^2}{\pi \langle p_T^2 \rangle}$	$\frac{\langle p_T^2(j) \rangle}{\langle p_T^2(f_1) \rangle}$
f_1	0.239	0.080	0.909	1
g_1	0.206	0.059	0.916	0.74
h_1	0.210	0.063	0.891	0.79
g_{1T}	0.206	0.059	0.916	0.74
$h_{1L}^\perp$	0.206	0.059	0.916	0.74
$h_{1T}^\perp$	0.190	0.050	0.919	0.63

Gaussian within such an accuracy. We make therefore the following second exercise.

We ask the question: what is the difference between computing in the model [78] an observable using exact model p_T dependence of TMDs and computing it by approximating the true p_T dependence by a Gaussian? We can rephrase this question also as follows: when integrating out the transverse momenta of produced hadrons and focusing, for example, on the x dependence of azimuthal asymmetries, the p_T-model dependence is weakened, but to what extent?

In order to answer that question we choose the double-spin asymmetry $A_{LT}^{\cos(\phi_h - \phi_S)}$ and use the model [84] for $D_1^a(z, K_T)$, which also refers to a low scale. (We stress that the results presented here are to be considered as an exploratory study of p_T-model effects. Our predictions for this asymmetry will be given in the subsequent section.)

In Fig. 4, we see the results for $A_{LT}^{\cos(\phi_h - \phi_S)}$ obtained as follows: The solid curve shows the result from solving numerically the convolution integral in (6) with $g_{1T}(x, p_T)$ from [78] and $D_1^a(z, K_T)$ from [84]. The dotted curve shows the result for the asymmetry obtained from the Gaussian model, Eq. (17), using $g_{1T}^{(1)a}(x)$ from [78] and $D_1^a(z)$ from [84], assuming the Gaussian Ansatz (15) for these functions, and assigning the Gaussian widths according to Eq. (38).

The different results agree within an accuracy of 20%, see Fig. 4. Such an uncertainty is "within the model accuracies" of Refs. [78,84]. Thus, we conclude that the true transverse-momentum dependence in the models [78,84] can be *approximated* by the Gaussian Ansatz with a satisfactory precision for practical purposes.
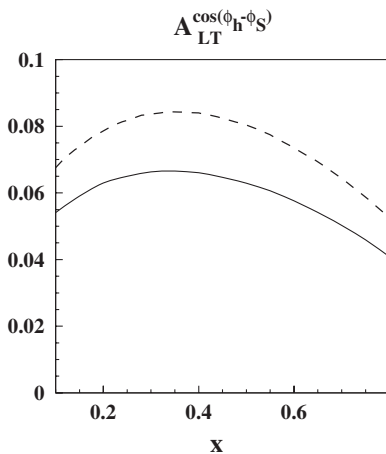
FIG. 4. $A_{LT}^{\cos(\phi_h - \phi_S)}$ in π^+ production off proton, as a function of x. Solid curve: exact result obtained using $g_{1T}(x, p_T)$ from [78] and $D_1(z, K_T)$ from [84]. Dashed curve: an approximation obtained using the integrated functions $g_{1T}^{(1)}(x)$, $D_1(z)$ from [78,84] and "simulating" their p_T dependence by means of the Gaussian Ansatz, as described in the text.

Next, we address the question how to use consistently the model predictions [78] for phenomenology—in view of the fact that they refer to a very low hadronic scale. The fact that $\langle p_T^2 \rangle$ of f_1^a in that model is smaller compared to what is required by phenomenology, Eq. (37), is perfectly reasonable. Sudakov effects make the p_T distributions broader, i.e., $\langle p_T^2 \rangle$ larger, when evolving to larger (experimentally relevant) scales.

This p_T broadening is expected to be independent of the quark polarization, in first approximation. Thus, what we can use for phenomenology are the model results for $\langle p_T^2 \rangle$ in units of the mean square transverse momenta of f_1, see last column in Table I, and take the "unit" $\langle p_T^2(f_1) \rangle$ from phenomenology, Eq. (37).

On the basis of the considerations in this and in the previous section, we are in the position to establish our strategy to treat azimuthal asymmetries in the following. Let us summarize.

(i) We will mainly focus on the x dependence of the asymmetries, especially in the valence-x region (see Sec. IV).

(ii) We will assume the Gaussian model, which is a reasonable approximation (this section, see above).

(iii) When information on a specific Gaussian width of a polarized TMD is needed, we will use the model prediction for the corresponding ratio (see last column in Table I), and the value from Eq. (37) for the width of f_1^a.

(iv) We will not discuss the z dependence of the azimuthal asymmetries, because here integrals over the x dependence enter which extend, depending on the experiment, to low-x regions where the model is not applicable.[1]

(v) Similar warnings apply to the $P_{h\perp}$ dependence of the asymmetries. We shall therefore address this point with particular care, see Sec. X below.

VI. THE DOUBLE-SPIN ASYMMETRY $A_{LT}^{\cos(\phi_h - \phi_S)}$

We start the discussion of azimuthal asymmetries with the double-spin asymmetry $A_{LT}^{\cos(\phi_h - \phi_S)} = F_{LT}^{\cos(\phi_h - \phi_S)} / F_{UU}$, which is proportional to $\sum_a e_a^2 g_{1T}^a D_1^a$, see Eq. (6). Assuming the Gaussian Ansatz, which gives a good approximation, see Sec. V, we have to model the prefactor B_0' in Eq. (17). For that let us rewrite that factor as

$$B_0' = \frac{\sqrt{\pi}M}{\langle p_T^2(f_1) \rangle^{1/2}} \left\{ \frac{\langle p_T^2(g_{1T}) \rangle}{\langle p_T^2(f_1) \rangle} + \frac{\langle K_T^2(D_1) \rangle}{z^2 \langle p_T^2(f_1) \rangle} \right\}^{-1/2}. \quad (40)$$

For the first ratio in the curly brackets we use the model

---

[1] We recall that the numerators and denominators of the asymmetries (5)–(10) are actually weighted by $1/Q^4 \propto 1/x^2$, which strongly emphasizes the role of the small-x region, whose description is beyond the range of applicability of the model.

prediction from the last column in Table I. For the second ratio in the curly brackets we use the numbers from Eq. (37).

Being interested in the x dependence of the asymmetry, we further integrate over z

$$A_{LT}^{\cos(\phi_h - \phi_S)}(x) = \frac{\sum_a e_a^2 x g_{1T}^{(1)a}(x)\langle B_0' D_1^a\rangle}{\sum_a e_a^2 x f_1^a(x)\langle D_1^a\rangle}, \qquad (41)$$

where $\langle\ldots\rangle$ denotes the average over z within the respective experimental cuts. Here and in the following, we will consider the range $0.2 \le z \le 0.7$ corresponding to the typical kinematics of HERMES. There is little difference if one uses the COMPASS cuts $0.2 \le z < 1$, since the resulting $\langle z\rangle$ is similar. At JLab typically higher $\langle z\rangle$ are reached. For the present observable, however, this has little impact.

The results for $A_{LT}^{\cos(\phi_h - \phi_S)}$ in DIS production of pions off different targets are shown in Fig. 5. For $g_{1T}^{(1)a}(x)$ and $f_1^a(x)$ we take the results from the model [78], and consider two options. First, we take both functions at the low scale of the model (dashed curves). Second, we consider both curves LO evolved to $Q^2 = 2.5$ GeV^2 (solid curves).

Hereby, we use for $g_{1T}^{(1)a}(x)$ the evolution equations for $g_1^a(x)$. This is admittedly not the correct evolution pattern. However, this is the evolution pattern of a chiral-even polarized function, and the purpose of presenting it here

is to shed some light on the possible size of evolution effects.

Our crude estimate of evolution effects indicates, that the predictions for the asymmetries are presumably robust concerning scale dependence. The proton asymmetries reach 4% in the valence-x region, which could be measured—especially at JLab. The deuteron asymmetries are somewhat smaller. For a deuteron target there also exist preliminary data from the 2002–2004 run of the COMPASS experiment [46]. As can be seen in Fig. 5, our results are compatible with these preliminary data.

Estimates for $A_{LT}^{\cos(\phi_h - \phi_S)}$ were made also in [67] on the basis of the approximation

$$g_{1T}^{(1)a}(x, Q^2) \overset{\text{WW}}{\approx} x\int_x^1 \frac{dy}{y} g_1^a(y, Q^2) \qquad (42)$$

using the parametrization [122] for $g_1^a(x)$. The approximation is "justified" in QCD upon the neglect of pure twist-3 (quark-gluon) correlators and current quark-mass terms [68–70]. This is analog to the Wandzura-Wilczek (WW) approximation for the twist-3 parton distribution function $g_T^a(x)$ [130–132]—hence, the label "WW" in (42). The WW approximation for $g_T^a(x)$ is supported experimentally within the error bars of the present data [133–135]. Whether the WW-type approximation (42) is supported by data equally well remains to be seen.

In the light-cone CQM [78] the "WW-type approximation," Eq. (42), is supported in the valence x region with good accuracy. Furthermore, our results support the find-
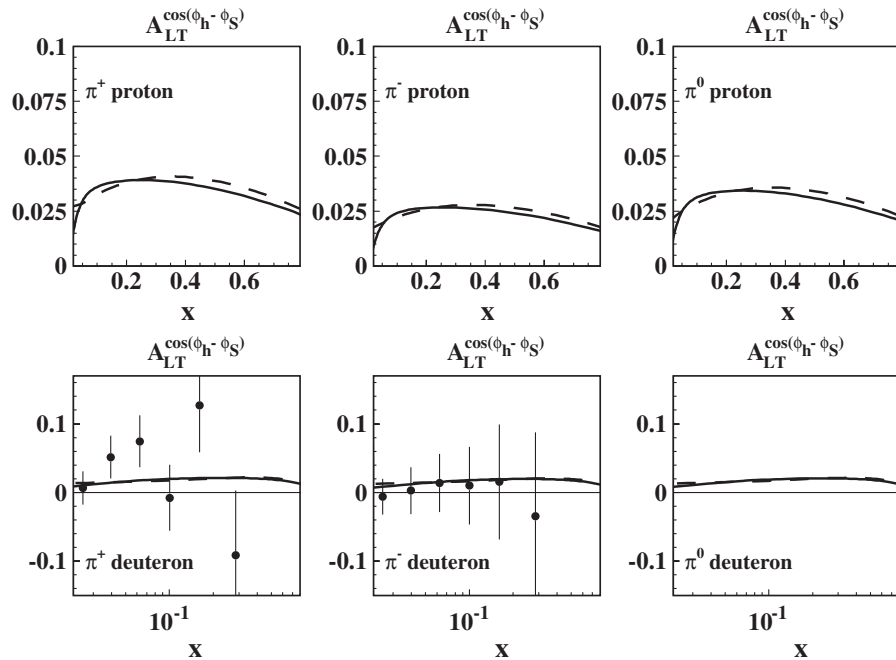
FIG. 5.   The double-spin asymmetry $A_{LT}^{\cos(\phi_h - \phi_S)}$ in DIS production of pions, as a function of x, obtained using $g_{1T}^{(1)a}(x)$ and $f_1^a(x)$ from the light-cone CQM [78] in the following way: both functions are taken at the low scale of the model (dashed curves), and both are LO evolved to $Q^2 = 2.5$ GeV^2 (solid curves). Hereby, the scale dependence of $g_{1T}^{(1)a}(x)$ is "simulated" using the $g_1^a(x)$ evolution pattern, see text. The data points are preliminary COMPASS data for charged hadron production off deuteron [46].

ings of [67] also numerically. Taking into account the different kinematical cuts applied in the calculation of [67], we obtain asymmetries of similar size, with a more flat x dependence.

VII. THE SINGLE-SPIN ASYMMETRY $A_{UT}^{\sin(\phi_h + \phi_S)}$

Next, we focus on the azimuthal single-spin asymmetry (SSA) $A_{UT}^{\sin(\phi_h + \phi_S)} = F_{UT}^{\sin(\phi_h + \phi_S)}/F_{UU}$ due to transversity and the Collins function. In the Gauss Ansatz (15) the structure function in the numerator of this SSA is given by the expression in Eq. (18).

For the Collins function, more precisely for $\langle B_1 H_1^{\perp(1/2)a}\rangle$ equal to $\langle 2B_{\text{Gauss}} H_1^{\perp(1/2)a}\rangle$ in the notation of [62], we use the results extracted in [62] from the (preliminary) HERMES data [38]. Although meanwhile new data are available [44,45,47,48] the results on $H_1^\perp$ from [62] are still in excellent agreement with updated extractions [64].

When dealing with asymmetries due to chiral-odd TMDs, in our opinion a different approach is more appropriate as compared to the case of asymmetries due to chiral-even TMDs. Let us explain this point in more detail.

When describing asymmetries due to chiral-even functions in the previous sections, we used model input for both the numerator and the denominator of the asymmetries. In the model gluon (and sea quark) degrees of freedom are absent at the low scale, and generated by evolution at higher scales. Admittedly, in this way one cannot accurately describe absolute DIS cross section data. For that nonzero unpolarized gluon and sea quark distributions are needed already at low input scales [121] (though the model scale is lower than the initial scale of the parametrizations [121]). This "shortcoming" of the model, however, affects similarly the numerator and the denominator of asymmetries due to chiral-even TMDs. Indeed, we observed that these model uncertainties partly cancel in the ratio—resulting in a useful description of (SI)DIS data on asymmetries in the valence-x region, see Sec. IV.

Can we expect a similarly good description of asymmetries, which are due to chiral-odd TMDs, using this strat-

egy? The answer is no, in our opinion. Transversity has no gluon counterpart, in contrast with $f_1^a(x)$. The absence of gluon degrees of freedom in an approach constitutes therefore a "lesser shortcoming" for $h_1^a(x)$ than for $f_1^a(x)$. So one expects intuitively that in quark models transversity and other chiral-odd TMDs could be modeled more reliably than chiral-even ones, though it is not clear how to put this expectation on a firm field theoretical basis.

Nevertheless, these considerations suggest to adopt the following strategy for the description of the Collins SSA, namely, to use $h_1^a(x)$ from the model LO evolved [56,136] to the experimental scale in the numerator of the SSA, and $f_1^a(x)$ from a parametrization, e.g., [121], taken at the corresponding scale. In this way, the model uncertainty is limited to the numerator of the SSA only, while the denominator is described exactly. We indeed observe that the above-described strategy yields by far the best results in the case of the Collins SSA, see Fig. 6. Any other options, such as $h_1^a(x)$ and $f_1^a(x)$ from the model at the low scale or $h_1^a(x)$ and $f_1^a(x)$ from the model LO evolved, gave unsatisfactory results.

Let us discuss in more detail the results for $A_{UT}^{\sin(\phi_h + \phi_S)}$ in Fig. 6, where for sake of clarity we refrain from showing the error bands due to the statistical and systematic uncertainties of the extracted Collins function [62]. Figures 6 (a) and 6(b) show the results for charged pion production from a proton target in comparison to the preliminary HERMES data [38]. (It is consistent to compare to these data, because the information on $H_1^\perp$ [62] was extracted from those data.) The model results ideally describe these data—including the small-x region, see Figs. 6(a) and 6(b). This is in line with the favorable comparison between our model predictions [56,104] and the phenomenological extraction of the transversity and tensor charges in Refs. [63,64].

In Figs. 6(c) and 6(d) we compare our results for $A_{UT}^{\sin\phi_C} \equiv -A_{UT}^{\sin(\phi_h + \phi_S)}$ (since $\phi_C = \phi_h + \phi_S + \pi$) for charged pion production from a deuterium target to the COMPASS data [47], which extend down to much lower values of x. Our
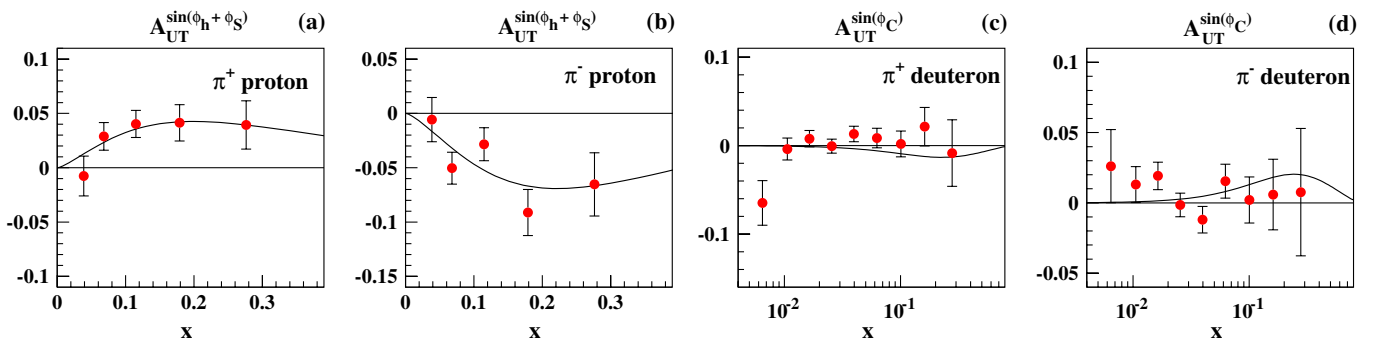
FIG. 6 (color online). The single-spin asymmetry $A_{UT}^{\sin(\phi_h + \phi_S)} \equiv -A_{UT}^{\sin\phi_C}$ in DIS production of charged pions off proton and deuteron targets, as a function of x. The theoretical curves are obtained on the basis of the light-cone CQM predictions for $h_1^a(x, Q^2)$ from Refs. [56,78], see text. The (preliminary) proton target data are from HERMES [38], the deuteron target data are from COMPASS [47].

results are compatible with the data also in this case, including again the small-x region.

On the basis of the presently available information on the Collins function extracted from SIDIS and e^+e^- data, we would predict π^0 SSAs compatible with zero within the uncertainties of the extractions [62–64]. However, this is a prediction due to our present understanding of the Collins effect, rather than due to the model for TMDs. For this reason, here and in the following two sections where we discuss further SSAs due to Collins effect, we refrain from showing results for neutral pion production.

VIII. THE SINGLE-SPIN ASYMMETRY $A_{UL}^{\sin(2\phi_h)}$

In this section we discuss the azimuthal SSA $A_{UL}^{\sin(2\phi_h)} = F_{UT}^{\sin(2\phi_h)}/F_{UU}$ due to $h_{1L}^{\perp a}$ and the Collins function. In the Gauss Ansatz (15) the structure function in the numerator of this SSA is given by the expression in Eq. (20). Thus, in order to describe this SSA we need $\langle B_2' H_1^{\perp(1/2)a}\rangle$, which we estimate on the basis of the Collins function extractions [57,59] precisely as described in Ref. [68].

The problem we face in the context of $A_{UL}^{\sin(2\phi_h)}$ concerns the question of how to evolve correctly $h_{1L}^{\perp(1)a}(x)$ from the low initial scale of the model to the relevant experimental scale. In contrast with transversity, exact evolution equations are not available in this case.

In our study of $A_{UT}^{\sin(\phi_h+\phi_S)}$ we learned that other strategies, such as leaving transversity at the low scale of the model [and taking $f_1^a(x)$ in the denominator from the model or from parametrization, at the low scale or evolved] resulted in unfavorable descriptions of data, and we were able to understand qualitatively why. Of course, this is here a different observable. But the experience with the Collins SSA does not encourage any other strategy than that adopted in that case, in Sec. VII, namely, to evolve the chiral-odd TMD from the model, and use parametrizations for the denominator of the SSA.

Not being able to evolve $h_{1L}^{\perp(1)a}(x)$ correctly we use instead the $h_1^a(x)$-evolution pattern to evolve it "approxi-

mately." Since both functions are chiral odd, the simulation of evolution effects in this way can be expected to be more promising than using any other evolution pattern.

In Fig. 7, we compare the results obtained in this way to the HERMES data from proton and deuteron targets [32,34]. We observe that our estimates are well compatible with the data—including again the small-x region. For comparison, in the Appendix and Ref. [137] we also show the results obtained with the same ingredients as in Fig. 7 but without approximate evolution of $h_{1L}^a(x)$. This approach yields a somewhat larger SSA, especially at large x, but it is similarly compatible with the data.

In Ref. [68] predictions for the $A_{UL}^{\sin(2\phi_h)}$ SSA were made on the basis of the WW-type approximation

$$h_{1L}^{\perp(1)a}(x) \overset{\text{WW}}{\approx} -x^2 \int_x^1 \frac{dy}{y^2} h_1^a(y), \qquad (43)$$

and model predictions for transversity from [138]. Equation (43) is analog to the approximation (42), i.e., it also arises when certain quark-gluon correlator and current quark-mass terms are neglected. Interestingly, the light-cone CQM supports the approximation (43) within a reasonable accuracy [78]. Also, the numerical results for the SSA obtained here and in [68] agree well qualitatively.

It is, of course, an important question how to quantify the theoretical uncertainty we introduced in our study by employing the incorrect evolution pattern for $h_{1L}^{\perp(1)a}(x)$. Until exact evolution equations for this TMD will be available, this question cannot be answered exactly. However, one may suspect that the uncertainties due to evolution are less dominating than other uncertainties within the model. The current HERMES data do not contradict this expectation, see Fig. 7. We remark that there are also preliminary CLAS data [41]. Our approach is compatible with the results for π^+ and π^0 but cannot explain the trend of the π^- SSA, similarly to Ref. [68]. The situation will be further clarified in future experiments at JLab [139,140], and COMPASS.
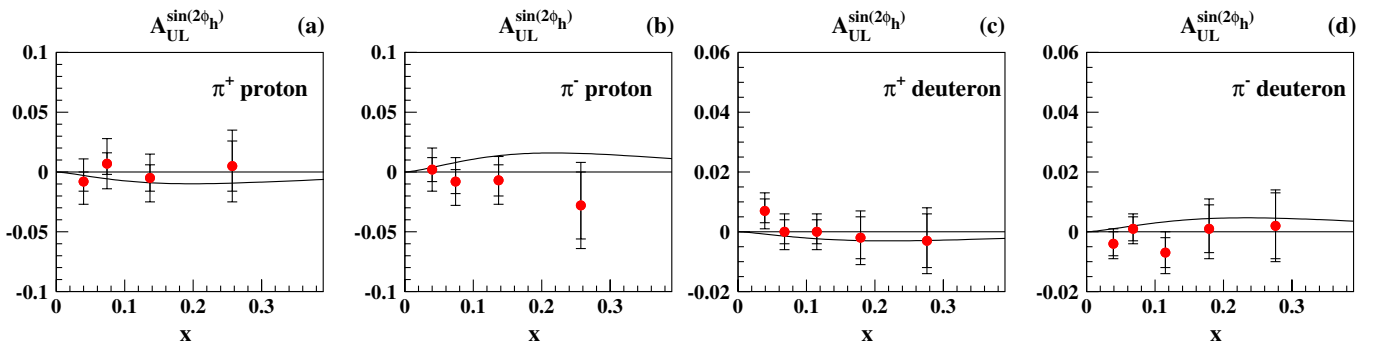
FIG. 7 (color online).   The single-spin asymmetry $A_{UL}^{\sin(2\phi_h)}$ in DIS production of charged pions off proton and deuteron targets, as a function of x. The theoretical curves are obtained by evolving the light-cone CQM predictions for $h_{1L}^{\perp(1)a}$ of Ref. [78] to $Q^2 = 2.5$ GeV^2, using the h_1^a evolution pattern, see text. The data points are from HERMES [32,34]. The inner error bars are the statistical errors, the outer error bars are the systematic errors.

IX. THE SINGLE-SPIN ASYMMETRY $A_{UT}^{\sin(3\phi_h-\phi_S)}$

Finally, we study the azimuthal SSA $A_{UT}^{\sin(3\phi_h-\phi_S)} = F_{UT}^{\sin(3\phi_h+\phi_S)}/F_{UU}$ due to pretzelosity and the Collins function. In the Gauss Ansatz (15) the structure function in the numerator of this SSA is given by the expression in Eq. (21). The factor $\langle B_3 H_1^{\perp(1/2)a}\rangle$ we evaluate exactly as done in Ref. [77].

Also in the context of the asymmetry $A_{UT}^{\sin(3\phi_h-\phi_S)}$ we face the question how to evolve $h_{1T}^{\perp(1)a}(x)$ from the low initial scale of the model to the relevant experimental scale. Exact evolution equations are not available in this case, either. We follow here the approach developed in the previous section, and "simulate" the evolution of $h_{1T}^{\perp(1)a}(x)$ by evolving it according to the transversity-evolution pattern. Again, since pretzelosity and transversity are chiral odd, this way might be a useful estimate of evolution effects.

The results obtained in this way are shown in Fig. 8. We find the pretzelosity SSA rather small, about 1% in the case of charged pions from a proton target, see Figs. 8(a) and 8(b). This makes it the probably most challenging asymmetry to be measured. The deuteron SSAs are somewhat smaller, see Figs. 8(c) and 8(d) where we show for comparison the preliminary COMPASS data presented in Ref. [46]. Our results are compatible with the data, and explain why the effect was found consistent with zero within error bars at COMPASS. The error bars of the preliminary data [46] simply do not allow to resolve an asymmetry smaller than 1%.

In Ref. [77] estimates for the asymmetry $A_{UT}^{\sin(3\phi_h-\phi_S)}$ were presented on the basis of the positivity bound $|h_{1T}^{\perp(1)a}(x)| \leq \frac{1}{2}(f_1^a(x) - g_1^a(x))$ [49], using the parametrizations [121] for $f_1^a(x)$, $g_1^a(x)$. The results of the light-cone CQM for pretzelosity (as well as other TMDs), of course, respect positivity bounds [78], and the transverse moment of pretzelosity at the low scale of the model is not that small, see Fig. 2. But after evolution (with the transversity-evolution pattern) to a scale of $Q^2 = 2.5$ GeV^2, it is much

smaller than its bound constructed from parameterizations for $f_1^a(x)$, $g_1^a(x)$ at $Q^2 = 2.5$ GeV^2. Therefore, our estimates of the pretzelosity SSA are significantly smaller than the maximal effect allowed by positivity requirements [77].

Of course, we do not know to which extent our approach to estimate the $h_{1T}^{\perp(1)}(x)$ evolution effects is really realistic. For comparison, in the Appendix and Ref. [137], we also make predictions neglecting the evolution of pretzelosity. In this way the results for the SSA are more sizable, and the effects are larger especially in the region of intermediate and large x. The planned experiment at JLab will allow us to discriminate among the different predictions [141].

X. $P_{h\perp}$-DEPENDENCE OF SPIN ASYMMETRIES

As discussed in Sec. V, care is required in order to use the model results for the p_T dependence of TMDs for phenomenological applications. In this section we shall exemplify how this can be done with a study of the $P_{h\perp}$ dependence of the double-spin asymmetry A_{LL}. In principle, we could discuss also other asymmetries, but A_{LL} has the advantage that its x and z dependence is rather well known—so we do not need the model input for that, and can focus on $P_{h\perp}$ dependence, which is the only new concept in this case. Would we discuss other (azimuthal) spin asymmetries, we would need to use the model input also for the x dependence of the novel TMD, and face the problems of how to evolve TMDs, make a meaningful estimate of Sudakov effects, and deal with the small-x region (see footnote [1]). When dealing with A_{LL} in the way described below, we avoid these problems.

Before discussing the $P_{h\perp}$ dependence of A_{LL} in our approach, let us remark that ideally a study of p_T effects should start with absolute cross section data on the production of hadrons in unpolarized DIS. Such data are difficult to produce, and experimentally it is preferable to study the $P_{h\perp}$ dependence of asymmetries, since detector acceptance effects in the numerator and denominator of the asymmetries (largely) cancel. Therefore, so far informa-
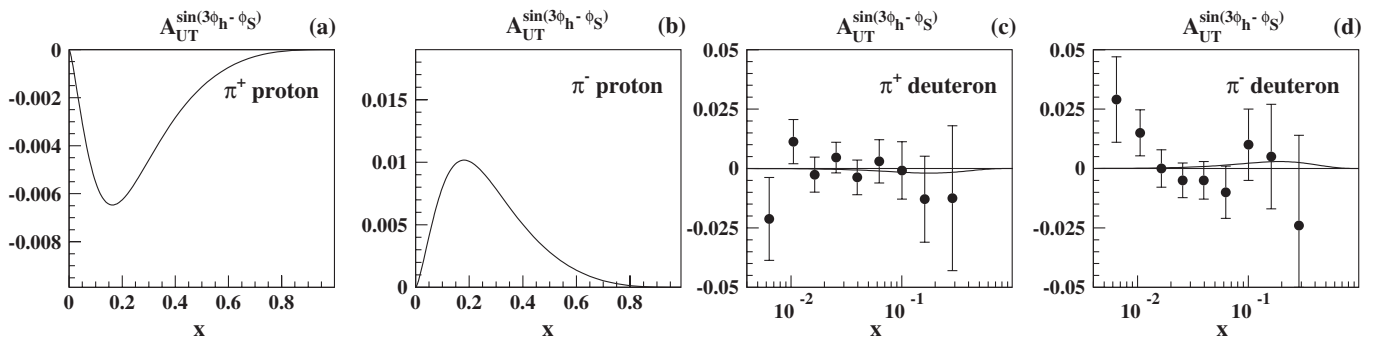
FIG. 8. The single-spin asymmetry $A_{UT}^{\sin(3\phi_h-\phi_S)}$ in DIS production of charged pions off proton and deuteron targets, as a function of x. The theoretical curves are obtained by evolving the light-cone CQM predictions for $h_{1T}^{\perp(1)a}$ of Ref. [78] to $Q^2 = 2.5$ GeV^2, using the h_1^a evolution pattern, see text. The preliminary COMPASS data are from Ref. [46].

tion from SIDIS on p_T dependence of the unpolarized parton distribution and fragmentation functions, f_1^a and D_1^a, has been obtained only indirectly, see Sec. V. It would be desirable to improve this situation. Apart from the absolute cross section proportional to F_{UU}, the next "simplest" observable to learn about p_T effects is probably $A_{LL} = F_{LL}/F_{UU}$.

In Sec. V, we learned that the Gauss Ansatz is supported within the model with reasonable accuracy. This justifies to make explicit use of it, also in this case. If we assume this Ansatz, then

$$F_{UU}(x, z, P_{h\perp}) = \sum_a e_a^2 x f_1^a(x) D_1^a(z) \frac{\exp(-P_{h\perp}^2/\langle P_{h\perp}^{2,\mathrm{unp}}\rangle)}{\pi \langle P_{h\perp}^{2,\mathrm{unp}}\rangle},$$

$$\langle P_{h\perp}^{2,\mathrm{unp}}\rangle = \langle K_T^2\rangle + z^2 \langle p_T^2(f_1)\rangle, \qquad (44)$$

$$F_{LL}(x, z, P_{h\perp}) = \sum_a e_a^2 x g_1^a(x) D_1^a(z) \frac{\exp(-P_{h\perp}^2/\langle P_{h\perp}^{2,\mathrm{pol}}\rangle)}{\pi \langle P_{h\perp}^{2,\mathrm{pol}}\rangle},$$

$$\langle P_{h\perp}^{2,\mathrm{pol}}\rangle = \langle K_T^2\rangle + z^2 \langle p_T^2(g_1)\rangle. \qquad (45)$$

If we assume that the widths are flavor and x or z independent, then the $P_{h\perp}$ dependence of the double-spin asymmetry is given by

$$A_{LL}(P_{h\perp}) = \langle A_{LL}\rangle \frac{\langle P_{h\perp}^{2,\mathrm{unp}}\rangle}{\langle P_{h\perp}^{2,\mathrm{pol}}\rangle} \exp\left[\frac{P_{h\perp}^2}{\langle P_{h\perp}^{2,\mathrm{unp}}\rangle} - \frac{P_{h\perp}^2}{\langle P_{h\perp}^{2,\mathrm{pol}}\rangle}\right], \qquad (46)$$

where $\langle A_{LL}\rangle$ denotes the spin asymmetry averaged over x and z, which is known in the experiment with precision. [Now, in Eq. (46) it is implied that "z^2" in (44) and (45) is replaced by $\langle z^2\rangle$. This is an approximation, and the treatment could be improved, but we refrain from this in our illustrative study for sake of clarity.]

We remark that positivity, i.e., $A_{LL} \leq 1 \ \forall \ x$ and $P_{h\perp}$, dictates

$$\frac{\langle p_T^2(g_1)\rangle}{\langle p_T^2(f_1)\rangle} \leq \left|\frac{g_1^a(x)}{f_1^a(x)}\right|. \qquad (47)$$

This implies that (in the Gauss Ansatz) the widths of helicity and the unpolarized distribution could be equal, if and only if the equality $f_1^a(x) = |g_1^a(x)|$ were true.

Now, let us discuss how to use the model results in order to predict the $P_{h\perp}$ dependence of A_{LL}. From Table I we know that

$$\frac{\langle p_T^2(g_1)\rangle}{\langle p_T^2(f_1)\rangle} = 0.74. \qquad (48)$$

If we take this ratio for granted, and assume for $\langle p_T^2(f_1)\rangle$ the result from [59], Eq. (37), then we obtain for $a(P_{h\perp}) \equiv A_{LL}(P_{h\perp})/\langle A_{LL}\rangle$ the results shown in Fig. 9. We include in Fig. 9 also predictions based on using the results for $\langle K_T^2\rangle$, $\langle p_T^2(f_1)\rangle$ from [57]. We observe a rather stable prediction,
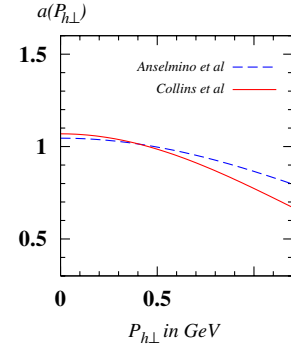
FIG. 9 (color online). $a(P_{h\perp}) \equiv A_{LL}(P_{h\perp})/\langle A_{LL}\rangle$ vs $P_{h\perp}$ in SIDIS, for experiments with $\langle z^2\rangle = 0.16$. The results are obtained using the prediction (48) from the model [78], and the Gauss model parameters in Eq. (37) from Ref. [59] (solid curve) or the corresponding parameters from Ref. [57] (dashed curve).

which depends little on the choice of parameters [59] vs [57]. The prediction in Fig. 9 depends more strongly on the model prediction (48).

This result is (in our approximations) the same for any target and produced hadron. In fact, in the SU(6) symmetric light-cone CQM of Ref. [78] the widths as defined in Eq. (38) are always flavor independent. But we recall, that the entire Gauss Ansatz is in the light of the results of Ref. [78] merely an approximation.

It will be instructive to learn to which extent our predictions will be confirmed by experiment. As mentioned, we could similarly discuss predictions from the model for azimuthal asymmetries, too. But those predictions would presumably have larger theoretical uncertainties, such that we shall content ourselves here with the study of the $P_{h\perp}$ dependence of A_{LL}.

XI. CONCLUSIONS

In this work we have studied all leading-twist azimuthal spin asymmetries in SIDIS due to T-even TMDs on the basis of predictions within one and the same model, i.e., the light-cone CQM of Ref. [78].

By studying first the well-known double-spin asymmetries A_1 in DIS and A_{LL} in SIDIS, we demonstrated that the approach is capable of describing the data on these asymmetries in the valence-x region with an accuracy of $\mathcal{O}(20–30)\%$. The comparison with results from other constituent models has shown this to be a typical accuracy to which the constituent quark model scenario can be expected to work.

We paid particular attention to the question, how to apply the model results for TMDs obtained at a very low hadronic scale to the description of data referring to high scales of typically several GeV^2. We made a test for the double-spin asymmetries A_1 in DIS and A_{LL} in SIDIS where the evolution equations involving the parton density $f_1^a(x)$ and the helicity distribution $g_1^a(x)$ are exactly known.

In these cases we have been able to demonstrate the stability under evolution of our results in the valence-x region.

For TMDs entering the description of azimuthal asymmetries, however, not only the evolution with renormalization scale has to be taken into account, but also Sudakov effects, which broaden the p_T distribution of the TMDs. We tackled this issue in two steps. First, we observed that the light-cone CQM [78] do not show a Gaussian p_T dependence. Nevertheless, their p_T dependence entering the azimuthal asymmetries is integrated over in certain convolution integrals, so that we have found that within the accuracy of our approach the effect of the true p_T dependence in the TMDs can be approximated by a Gaussian dependence. We have therefore explicitly employed the Gaussian Ansatz, which allows to express azimuthal asymmetries in terms of parton distribution functions or transverse moments of TMDs. In the second step, we used evolution equations to evolve the respective parton distribution functions or transverse moments of TMDs to the experimental scales.

We have been able to do this *exactly*, strictly speaking, only in the case of transversity $h_1^a(x)$. In the other cases, the evolution of the transverse moments of TMDs was estimated by employing those evolution equations, which seem most promising to be able to simulate the correct evolution, which is presently not available. For example, we evolved $g_{1T}^{(1)a}(x)$ by means of the evolution pattern of the (also chiral even) $g_1^a(x)$, while for $h_{1L}^{\perp(1)a}(x)$, $h_{1T}^{\perp(1)a}(x)$ we used the evolution pattern of the chiral odd $h_1^a(x)$. The theoretical uncertainties due to these approximate treatment of the scale dependence are presumably not larger than the accuracy of the model.

Among the leading-twist azimuthal spin asymmetries due to T-even TMDs, the Collins SSA $A_{UT}^{\sin(\phi_h+\phi_S)}$ is the only nonzero one within the present day error bars. We observe a very good agreement of our results for the x dependence of this SSA with the HERMES proton [36,38], as well as with the COMPASS deuteron target data [37,40].

The presently available final data on $A_{UL}^{\sin(2\phi_h)}$ [32,34] or preliminary data on $A_{LT}^{\cos(\phi_h-\phi_S)}$ and $A_{UT}^{\sin(3\phi_h-\phi_S)}$ [46] show results compatible with zero within error bars. Our results are compatible with these first or preliminary data. In future, our predictions of these azimuthal spin asymmetries could be tested by more precise data—especially from COMPASS and JLab.

In an exploratory study of the double-spin asymmetry A_{LL} we have shown how model results for TMDs obtained at very low scale could be applied for studies of the $P_{h\perp}$ dependence of spin asymmetries. We have chosen this observable, because here the $P_{h\perp}$ dependence is the only new aspect, the x and z dependence being known experimentally with good precision. For that we explored again the fact that the light-cone CQM [78] supports the Gaussian Ansatz for TMDs within a reasonable accuracy, and used as model input only the prediction for the ratio of the mean transverse-momentum squares of g_1^a and f_1^a. This ratio is expected to be little affected by Sudakov effects in a first approximation. We made predictions for $A_{LL}(P_{h\perp})$, which could be tested soon, for example, at JLab [141].

The advantage of our study is that the same model input has been used to describe all leading-twist spin asymmetries due to T-even TMDs. Wherever the data allow to draw definite conclusions, we observed a good agreement with the experiment in the range of applicability of the approach. It remains to be seen whether also our predictions for the other azimuthal spin asymmetries will be similarly confirmed by future data. If so, our approach will provide interesting insights in the spin and orbital angular momentum structure of the nucleon, which—though being model dependent—are of interest by themselves, as it is exposed in the Appendix.

APPENDIX: ANGULAR MOMENTUM DECOMPOSITION OF SPIN ASYMMETRIES

In this Appendix we discuss the contribution from the different angular momentum components of the nucleon wave function to the spin asymmetries. To this aim, we calculate the numerator of the asymmetries using the results of the TMDs at the hadronic scale of the model, and separating them into partial wave contributions according to the decomposition shown in Fig. 2 of Sec. III. In order to discuss how this decomposition behaves under evolution to higher scale, one would need to know the evolution equations for the different angular momentum components of the nucleon wave function separately, but, to our knowledge, this problem has never been addressed so far and is beyond the scope of our work. Although this decomposition is model dependent and it is not possible to extract experimentally the absolute strength of the different partial waves, it is instructive to visualize how the angular momentum content of the TMDs affects the spin asymmetries. In particular, the combined analysis of different spin asymmetries can give insights about the relative strength of the different partial waves, and therefore can be useful in modeling the light-cone wave function of the nucleon.
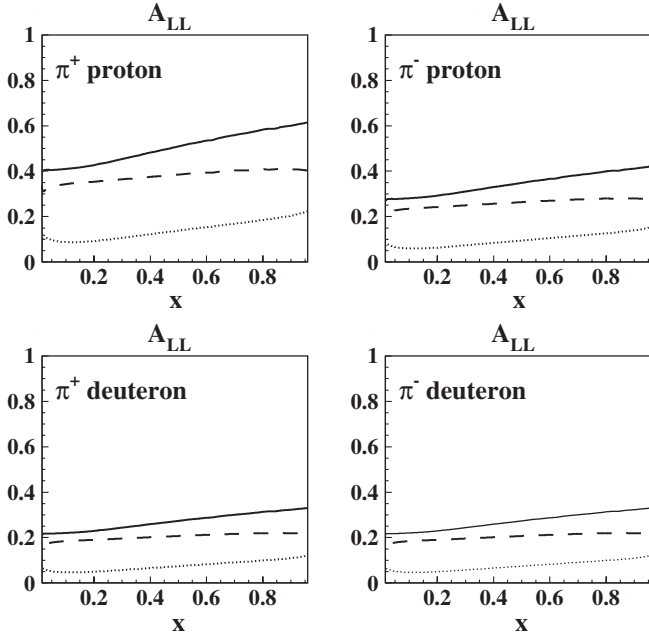
FIG. 10.   The double-spin asymmetry A_{LL} in DIS production of charged pions off proton and deuteron targets, as a function of x. The results are obtained using $g_1^a(x)$ and $f_1^a(x)$ from the light-cone CQM [78] at the hadronic scale, and decomposing $g_1^a(x)$ into different partial-wave contributions: the dashed curves correspond to the contribution from S waves, the dotted curves are the results for the P-wave contribution, and the solid curves are the total results.

The results for the SSAs presented in this Appendix, correspond to an alternative approach concerning the question how to use the model results referring to a low hadronic scale for phenomenology at experimentally relevant scales. Namely, here we use the model at the low scale only as input for the part which is responsible for the spin effects. For the well-known denominator of the SSAs, we use standard parametrizations at the experimental scale. In this way, the model uncertainty is only in the numerator. The comparison of these results and those presented in Secs. VI, VIII, and IX, where attempts were made to approximate evolution effects of the TMDs, with forthcoming experimental data [139–141] may give us interesting information about the scale dependence of these observables.

In Fig. 10, we show the results for the A_{LL} asymmetry, obtained by using both the unpolarized distribution function f_1 and the helicity distribution function g_1 from the light-cone CQM at low scale. The total results are further split into the contributions to g_1 from the S- (dashed curve) and P-wave (dotted curve) components, while the D-wave contribution is not shown because it is negligible. These separate terms reflect the dominance of the S-wave component with respect to the P wave in g_1, as already observed in Fig. 2 of Sec. III. Furthermore, the S-wave term is practically constant in the full x range, while the P-wave contribution is slowly increasing at a larger value of x, reaching a maximum of about 30% of the total result.

The $A_{LT}^{\cos(\phi_h - \phi_S)}$ asymmetry shown in Fig. 11 is calculated with both the unpolarized distribution function f_1
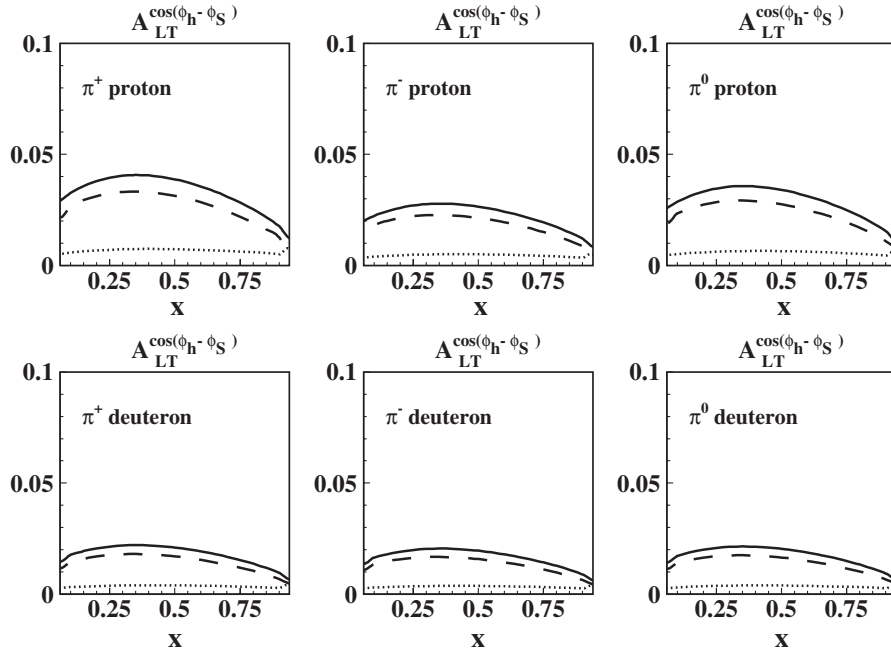
FIG. 11.   The double-spin asymmetry $A_{LT}^{\cos(\phi_h-\phi_S)}$ in DIS production of pions off proton and deuteron targets, as a function of x. The results are obtained using $g_{1T}^{(1)a}(x)$ and $f_1^a(x)$ from the light-cone CQM [78] at the hadronic scale, and decomposing $g_{1T}^{(1)a}$ into different partial-wave contributions: the dashed curves correspond to the contribution from the S- and P-wave interference, the dotted curves are the results for the P- and D-wave interference term, and the solid curves are the total results.
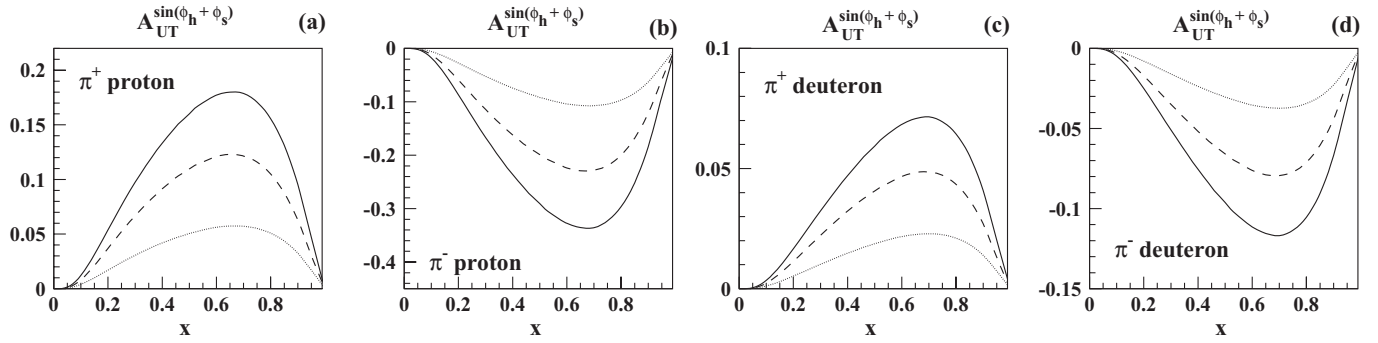
FIG. 12. The single-spin asymmetry $A_{UT}^{\sin(\phi_h + \phi_S)}$ in DIS production of charged pions off proton and deuteron targets, as a function of x. The results are obtained using the parametrization of Ref. [121] for $f_1^a(x)$ at $Q^2 = 2.5$ GeV^2, and the light-cone CQM predictions for $h_1^a(x)$ at the hadronic scale from Refs. [56,78]. The dashed and dotted curves are obtained separating the contributions to $h_1^a(x)$ from S and P waves, respectively. The solid curves show the total results, sum of the S- and P-wave contributions.

and the helicity distribution function $g_{1T}^{(1)}$ from the light-cone CQM at low scale. Here, we separate the contribution to $g_{1T}^{(1)}$ from the interference of S and P waves (dashed curves) and from the interference of P and D waves (dotted curves). We see that the S- and P-wave interference term governs both the size and the shape in x of the total results, while the contribution of the P- and D-wave interference is rather small and constant in the full x range.

We now pass to consider single-spin asymmetries involving chiral-odd TMDs. In the following, we will use for f_1 the parametrization from Ref. [121] at $Q^2 = 2.5$ GeV^2, while for the h_1, $h_{1T}^{(1)\perp}$, and $h_{1L}^{(1)\perp}$ TMDs we will use the results from the light-cone CQM at low scale. The $A_{UT}^{\sin(\phi_h + \phi_S)}$ asymmetry is shown in Fig. 12, with the separate contribution to h_1 from the S- (dashed curves) and P-wave (dotted curves) components. The contribution from the P waves is within 30% of the total results, and, at variance with the double-spin asymmetries discussed above, the two partial-wave contributions have very similar x dependence, with a maximum at $x \simeq 0.7$.

In Fig. 13, we show the results for the $A_{UL}^{\sin(2\phi_h)}$ asymmetry, due to the to the $h_{1L}^{\perp}$ TMD. Since in our model $h_{1L}^{\perp} = -g_{1T}$, the relative strength of the contributions from the S- and P-wave interference (dashed curves) and the P- and D-wave interference (dotted curves) is the same as for the corresponding contributions in $A_{LT}^{\cos(\phi_h - \phi_S)}$.

Finally, in Fig. 14, we show the results for the $A_{UT}^{\sin(3\phi_h + \phi_S)}$ asymmetry, separating the contributions to $h_{1T}^{(1)\perp}$ from the interference of P waves (dashed curves) and S-D waves (dotted curves). This is the only case where we can exploit the interference with the large S-wave contribution to amplify the effects due to the small D wave. The two interference terms have a quite different shape as a function of x: in the case of the P-wave interference, we have an oscillating behavior, with a sign change at $x \simeq 0.7$, while the S-D wave interference term is similar to a bell-shaped curve with the maximum at $x \simeq 0.7$. The sum of these two contributions gives a total result, which is peaked at $x \simeq 0.4$. At larger x, the S-D wave interference term gives the main contribution, while at smaller x the P wave and the S-D wave interference terms contribute with the same strength.
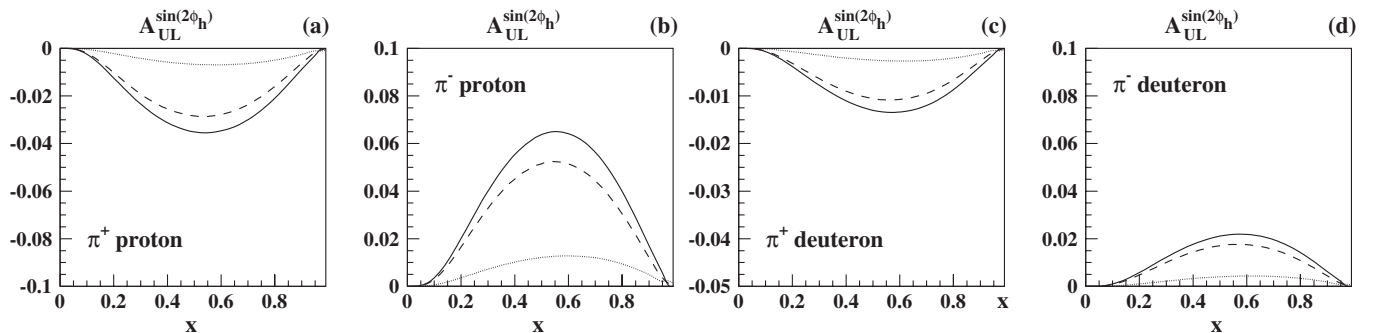
FIG. 13. The contribution from different angular momentum components to the single-spin asymmetry $A_{UL}^{\sin(2\phi_h)}$ in DIS production of charged pions off proton and deuteron targets, as a function of x. The results are obtained using the light-cone CQM predictions for $h_{1L}^{(1)\perp a}(x)$ at the hadronic scale and the parametrization of Ref. [121] for $f_1^a(x)$ at $Q^2 = 2.5$ GeV^2. The dashed and dotted curves are obtained separating the contributions to $h_{1L}^{(1)\perp a}(x)$ from the interference of S- and P-wave components and from the interference of P- and D-wave components, respectively. The solid curves correspond to the total results.
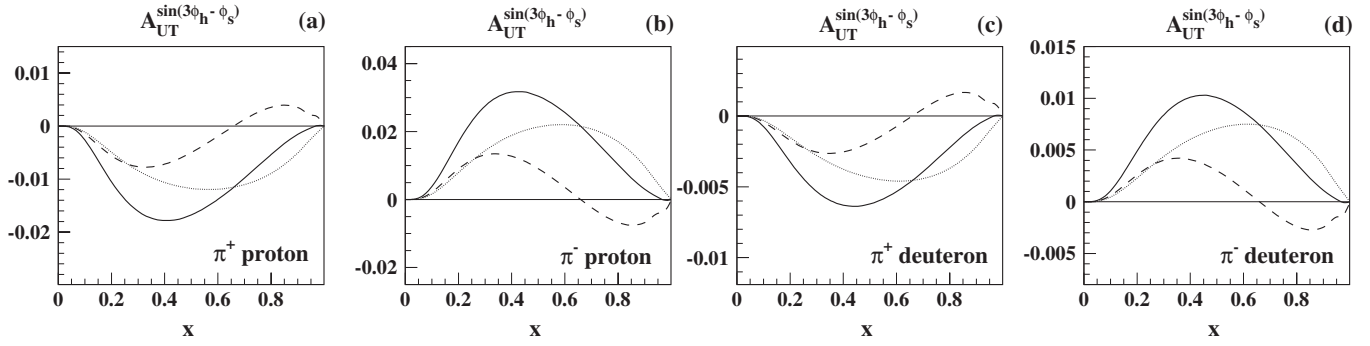
FIG. 14. The contribution from different angular momentum components to the single-spin asymmetry $A_{UT}^{\sin(3\phi_h - \phi_S)}$ in DIS production of charged pions off proton and deuteron targets, as a function of x. The results are obtained using the light-cone CQM predictions for $h_{1T}^{(1)\perp a}(x)$ at the hadronic scale and the parametrization of Ref. [121] for $f_1^a(x)$ at $Q^2 = 2.5$ GeV^2. The dashed and dotted curves are obtained separating the contributions to $h_{1T}^{(1)\perp a}(x)$ from the interference of $L_z = +1$ and $L_z = -1$ angular momentum components, and from the interference of $L_z = 0$ and $L_z = +2$ angular momentum components, respectively. Solid curves: total results.

[1] J. C. Collins, Acta Phys. Pol. B **34**, 3103 (2003).

[2] J. C. Collins, T. C. Rogers, and A. M. Stasto, Phys. Rev. D **77**, 085009 (2008).

[3] D. Boer and P. J. Mulders, Phys. Rev. D **57**, 5780 (1998).

[4] D. W. Sivers, Phys. Rev. D **41**, 83 (1990); Phys. Rev. D **43**, 261 (1991).

[5] R. N. Cahn, Phys. Lett. **78B**, 269 (1978).

[6] J. C. Collins, D. E. Soper, and G. Sterman, Nucl. Phys. **B250**, 199 (1985).

[7] A. V. Efremov, L. Mankiewicz, and N. A. Tornqvist, Phys. Lett. B **284**, 394 (1992).

[8] J. C. Collins, Nucl. Phys. **B396**, 161 (1993).

[9] J. C. Collins, S. F. Heppelmann, and G. A. Ladinsky, Nucl. Phys. **B420**, 565 (1994).

[10] A. Kotzinian, Nucl. Phys. **B441**, 234 (1995).

[11] P. J. Mulders and R. D. Tangerman, Nucl. Phys. **B461**, 197 (1996); **B484**, 538(E) (1997).

[12] D. Boer, R. Jakob, and P. J. Mulders, Nucl. Phys. **B504**, 345 (1997).

[13] D. Boer, Phys. Rev. D **60**, 014012 (1999).

[14] S. J. Brodsky, D. S. Hwang, and I. Schmidt, Phys. Lett. B **530**, 99 (2002); Nucl. Phys. **B642**, 344 (2002).

[15] J. C. Collins, Phys. Lett. B **536**, 43 (2002).

[16] A. V. Belitsky, X. Ji, and F. Yuan, Nucl. Phys. **B656**, 165 (2003); X. D. Ji and F. Yuan, Phys. Lett. B **543**, 66 (2002); D. Boer, P. J. Mulders, and F. Pijlman, Nucl. Phys. **B667**, 201 (2003).

[17] A. Bacchetta, P. J. Mulders, and F. Pijlman, Phys. Lett. B **595**, 309 (2004).

[18] I. O. Cherednikov and N. G. Stefanis, Phys. Rev. D **77**, 094001 (2008); Nucl. Phys. **B802**, 146 (2008).

[19] K. Goeke, A. Metz, and M. Schlegel, Phys. Lett. B **618**, 90 (2005).

[20] U. D'Alesio and F. Murgia, Prog. Part. Nucl. Phys. **61**, 394 (2008).

[21] V. Barone, A. Drago, and P. G. Ratcliffe, Phys. Rep. **359**, 1 (2002).

[22] A. V. Efremov and A. V. Radyushkin, Theor. Math. Phys. **44**, (1981)[Teor. Mat. Fiz. **44**, 157 (1980)].

[23] J. C. Collins and D. E. Soper, Nucl. Phys. **B193**, 381 (1981); **B213**, 545(E) (1983).

[24] X. D. Ji, J. P. Ma, and F. Yuan, Phys. Rev. D **71**, 034005 (2005); Phys. Lett. B **597**, 299 (2004).

[25] J. C. Collins and A. Metz, Phys. Rev. Lett. **93**, 252001 (2004).

[26] A. Bacchetta, M. Diehl, K. Goeke, A. Metz, P. J. Mulders, and M. Schlegel, J. High Energy Phys. 02 (2007) 093.

[27] M. Diehl and S. Sapeta, Eur. Phys. J. C **41**, 515 (2005).

[28] N. Dombey, Rev. Mod. Phys. **41**, 236 (1969).

[29] M. Gourdin, Nucl. Phys. **49**, 501 (1972).

[30] S. Boffi, C. Giusti, and F. D. Pacati, Phys. Rep. **226**, 1 (1993).

[31] M. Arneodo et al. (European Muon Collaboration), Z. Phys. C **34**, 277 (1987).

[32] A. Airapetian et al. (HERMES Collaboration), Phys. Rev. Lett. **84**, 4047 (2000); H. Avakian (HERMES Collaboration), Nucl. Phys. B, Proc. Suppl. **79**, 523 (1999).

[33] A. Airapetian et al. (HERMES Collaboration), Phys. Rev. D **64**, 097101 (2001).

[34] A. Airapetian et al. (HERMES Collaboration), Phys. Lett. B **562**, 182 (2003).

[35] H. Avakian et al. (CLAS Collaboration), Phys. Rev. D **69**, 112004 (2004).

[36] A. Airapetian et al. (HERMES Collaboration), Phys. Rev. Lett. **94**, 012002 (2005).

[37] V. Y. Alexakhin et al. (COMPASS Collaboration), Phys. Rev. Lett. **94**, 202002 (2005).

[38] M. Diefenthaler (HERMES Collaboration), AIP Conf. Proc. **792**, 933 (2005); L. L. Pappalardo (HERMES Collaboration), Eur. Phys. J. A **38**, 145 (2008).

[39] I. M. Gregor (HERMES Collaboration), Acta Phys. Pol. B **36**, 209 (2005).

[40] E. S. Ageev et al. (COMPASS Collaboration), Nucl. Phys. **B765**, 31 (2007); A. Martin (COMPASS Collaboration), Czech. J. Phys. **56**, F33 (2006).

[41] H. Avakian, P. Bosted, V. Burkert, and L. Elouadrhiri (CLAS Collaboration), AIP Conf. Proc. **792**, 945 (2005).

[42] A. Airapetian *et al.* (HERMES Collaboration), Phys. Lett. B **622**, 14 (2005).

[43] A. Airapetian *et al.* (HERMES Collaboration), Phys. Lett. B **648**, 164 (2007).

[44] K. Abe *et al.* (Belle Collaboration), Phys. Rev. Lett. **96**, 232002 (2006).

[45] M. Diefenthaler (HERMES Collaboration), arXiv:0706.2242; AIP Conf. Proc. **915**, 509 (2007).

[46] A. Kotzinian (on behalf of the COMPASS Collaboration), arXiv:0705.2402.

[47] M. Alekseev *et al.* (COMPASS Collaboration), Phys. Lett. B **673**, 127 (2009).

[48] R. Seidl, M. Grosse-Perdekamp, and A. Ogawa (Belle Collaboration), Phys. Rev. D **78**, 032011 (2008).

[49] A. Bacchetta, M. Boglione, A. Henneman, and P. J. Mulders, Phys. Rev. Lett. **85**, 712 (2000).

[50] A. Bacchetta, R. Kundu, A. Metz, and P. J. Mulders, Phys. Rev. D **65**, 094021 (2002).

[51] A. V. Efremov and P. Schweitzer, J. High Energy Phys. 08 (2003) 006.

[52] A. V. Efremov, K. Goeke, and P. Schweitzer, Eur. Phys. J. C **32**, 337 (2003).

[53] U. D'Alesio and F. Murgia, Phys. Rev. D **70**, 074009 (2004).

[54] M. Anselmino, V. Barone, A. Drago, and N. N. Nikolaev, Phys. Lett. B **594**, 97 (2004).

[55] A. V. Efremov, K. Goeke, and P. Schweitzer, Eur. Phys. J. C **35**, 207 (2004).

[56] B. Pasquini, M. Pincetti, and S. Boffi, Phys. Rev. D **76**, 034020 (2007).

[57] M. Anselmino, M. Boglione, U. D'Alesio, A. Kotzinian, F. Murgia, and A. Prokudin, Phys. Rev. D **71**, 074006 (2005).

[58] A. V. Efremov, K. Goeke, S. Menzel, A. Metz, and P. Schweitzer, Phys. Lett. B **612**, 233 (2005).

[59] J. C. Collins, A. V. Efremov, K. Goeke, S. Menzel, A. Metz, and P. Schweitzer, Phys. Rev. D **73**, 014021 (2006).

[60] J. C. Collins *et al.*, Phys. Rev. D **73**, 094023 (2006).

[61] W. Vogelsang and F. Yuan, Phys. Rev. D **72**, 054028 (2005).

[62] A. V. Efremov, K. Goeke, and P. Schweitzer, Phys. Rev. D **73**, 094025 (2006).

[63] M. Anselmino, M. Boglione, U. D'Alesio, A. Kotzinian, F. Murgia, A. Prokudin, and C. Turk, Phys. Rev. D **75**, 054032 (2007).

[64] M. Anselmino, M. Boglione, U. D'Alesio, A. Kotzinian, F. Murgia, A. Prokudin, and S. Melis, arXiv:0812.4366.

[65] S. Arnold, A. V. Efremov, K. Goeke, M. Schlegel, and P. Schweitzer, arXiv:0805.2137.

[66] M. Anselmino *et al.*, Eur. Phys. J. A **39**, 89 (2009).

[67] A. Kotzinian, B. Parsamyan, and A. Prokudin, Phys. Rev. D **73**, 114017 (2006).

[68] H. Avakian, A. V. Efremov, K. Goeke, A. Metz, P. Schweitzer, and T. Teckentrup, Phys. Rev. D **77**, 014023 (2008).

[69] A. Metz, P. Schweitzer, and T. Teckentrup, arXiv:0810.5212.

[70] H. Avakian, A. V. Efremov, P. Schweitzer, A. Metz, and T. Teckentrup, arXiv:0902.0689.

[71] H. Avakian, S. J. Brodsky, A. Deur, and F. Yuan, Phys. Rev. Lett. **99**, 082001 (2007).

[72] S. J. Brodsky and F. Yuan, Phys. Rev. D **74**, 094018

(2006).

[73] M. Burkardt, arXiv:0709.2966; G. A. Miller, Phys. Rev. C **76**, 065209 (2007).

[74] P. V. Pobylitsa, arXiv:hep-ph/0301236.

[75] F. Yuan, Phys. Lett. B **575**, 45 (2003).

[76] R. Jakob, P. J. Mulders, and J. Rodrigues, Nucl. Phys. **A626**, 937 (1997); *Proc. Int. Conf. on Perspectives in Hadronic Physics*, edited by S. Boffi, C. Ciofi degli Atti, and M. Giannini (World Scientific, Singapore, 1998), p. 320.

[77] H. Avakian, A. V. Efremov, P. Schweitzer, and F. Yuan, Phys. Rev. D **78**, 114024 (2008).

[78] B. Pasquini, S. Cazzaniga, and S. Boffi, Phys. Rev. D **78**, 034025 (2008).

[79] A. Bacchetta, F. Conti, and M. Radici, Phys. Rev. D **78**, 074010 (2008).

[80] J. She, J. Zhu, and B. Q. Ma, Phys. Rev. D **79**, 054008 (2009).

[81] S. Meissner, A. Metz, and K. Goeke, Phys. Rev. D **76**, 034002 (2007).

[82] A. V. Efremov, P. Schweitzer, O. V. Teryaev, and P. Zavada, arXiv:0812.3246.

[83] L. P. Gamberg, G. R. Goldstein, and M. Schlegel, Phys. Rev. D **77**, 094016 (2008); arXiv:0708.2580.

[84] A. Bacchetta, L. P. Gamberg, G. R. Goldstein, and A. Mukherjee, Phys. Lett. B **659**, 234 (2008).

[85] A. Courtoy, F. Fratini, S. Scopetta, and V. Vento, Phys. Rev. D **78**, 034002 (2008).

[86] A. Courtoy, S. Scopetta, and V. Vento, Phys. Rev. D **79**, 074001 (2009).

[87] A. Kotzinian, arXiv:0806.3804.

[88] B. Pasquini and S. Boffi, Phys. Rev. D **76**, 074011 (2007).

[89] S. Boffi and B. Pasquini, Riv. Nuovo Cimento Soc. Ital. Fis. **30**, 387 (2007).

[90] F. Landry, R. Brock, P. M. Nadolsky, and C. P. Yuan, Phys. Rev. D **67**, 073016 (2003).

[91] S. D. Drell and T. Yan, Phys. Rev. Lett. **24**, 181 (1970); G. B. West, Phys. Rev. Lett. **24**, 1206 (1970).

[92] M. Diehl, T. Feldmann, R. Jakob, and P. Kroll, Nucl. Phys. **B596**, 33 (2001); **B605**, 647(E) (2001); S. J. Brodsky, M. Diehl, and D. S. Hwang, Nucl. Phys. **B596**, 99 (2001).

[93] S. Boffi, B. Pasquini, and M. Traini, Nucl. Phys. **B649**, 243 (2003).

[94] X. d. Ji, J. P. Ma, and F. Yuan, Nucl. Phys. **B652**, 383 (2003).

[95] G. P. Lepage and S. J. Brodsky, Phys. Rev. D **22**, 2157 (1980).

[96] V. L. Chernyak and A. R. Zhitnitsky, Phys. Rep. **112**, 173 (1984).

[97] I. D. King and C. T. Sachrajda, Nucl. Phys. **B279**, 785 (1987).

[98] V. L. Chernyak, A. A. Ogloblin, and I. R. Zhitnitsky, Yad. Fiz. **48**, 1410 (1988) [Z. Phys. C **42**, 569 (1989)]; Sov. J. Nucl. Phys. **48** 896 (1988).

[99] V. M. Braun, S. E. Derkachov, G. P. Korchemsky, and A. N. Manashov, Nucl. Phys. **B553**, 355 (1999).

[100] V. Braun, R. J. Fries, N. Mahnke, and E. Stein, Nucl. Phys. **B589**, 381 (2000); **607**, 433(E) (2001).

[101] N. G. Stefanis, Eur. Phys. J. direct C **7**, 1 (1999).

[102] M. Burkardt, X. d. Ji, and F. Yuan, Phys. Lett. B **545**, 345 (2002).

[103] X. Ji, J.-P. Ma, and F. Yuan, Eur. Phys. J. C **33**, 75 (2004); Phys. Rev. Lett. **90**, 241601 (2003).

[104] B. Pasquini, M. Pincetti, and S. Boffi, Phys. Rev. D **72**, 094029 (2005).

[105] F. Schlumpf, arXiv:hep-ph/9211255.

[106] F. Schlumpf, J. Phys. G **20**, 237 (1994); Phys. Rev. D **47**, 4114 (1993); **49**, 6246(E) (1994); S. J. Brodsky and F. Schlumpf, Phys. Lett. B **329**, 111 (1994),

[107] P. Faccioli, M. Traini, and V. Vento, Nucl. Phys. **A656**, 400 (1999).

[108] M. Ferraris, M. M. Giannini, M. Pizzo, E. Santopinto, and L. Tiator, Phys. Lett. B **364**, 231 (1995).

[109] M. Traini, V. Vento, A. Mair, and A. Zambarda, Nucl. Phys. A **614**, 472 (1997); A. Mair and M. Traini, Nucl. Phys. **A624**, 564 (1997); **A628**, 296 (1998).

[110] S. Boffi, B. Pasquini, and M. Traini, Nucl. Phys. **B680**, 147 (2004).

[111] S. Scopetta, V. Vento, and M. Traini, Phys. Lett. B **421**, 64 (1998); **442**, 28 (1998).

[112] W. Broniowski, E. R. Arriola, and K. Golec-Biernat, Phys. Rev. D **77**, 034023 (2008).

[113] B. Pasquini, M. Traini, and S. Boffi, Phys. Rev. D **71**, 034022 (2005).

[114] M. Miyama and S. Kumano, Comput. Phys. Commun. **94**, 185 (1996).

[115] M. Hirai, S. Kumano, and M. Miyama, Comput. Phys. Commun. **108**, 38 (1998).

[116] A. V. Kotikov and D. V. Peshekhonov, Yad. Fiz. **60**, 736 (1997) [Phys. At. Nucl. **60**, 653 (1997)]; Eur. Phys. J. C **9**, 55 (1999).

[117] K. Abe *et al.* (E143 Collaboration), Phys. Rev. D **58**, 112003 (1998).

[118] J. Ashman *et al.* (European Muon Collaboration), Phys. Lett. B **206**, 364 (1988).

[119] B. Adeva *et al.* (Spin Muon Collaboration), Phys. Rev. D **60**, 072004 (1999); **62**, 079902(E) (2000).

[120] S. Kretzer, Phys. Rev. D **62**, 054001 (2000).

[121] M. Glück, E. Reya, and A. Vogt, Eur. Phys. J. C **5**, 461 (1998).

[122] M. Glück, E. Reya, M. Stratmann, and W. Vogelsang, Phys. Rev. D **63**, 094005 (2001).

[123] X. Zheng *et al.* (Jefferson Lab Hall A Collaboration), Phys. Rev. Lett. **92**, 012004 (2004); Phys. Rev. C **70**, 065207 (2004).

[124] K. V. Dharmawardane *et al.* (CLAS Collaboration), Phys. Lett. B **641**, 11 (2006).

[125] P. L. Anthony *et al.* (E142 Collaboration), Phys. Rev. D **54**, 6620 (1996).

[126] K. Abe *et al.* (E154 Collaboration), Phys. Lett. B **405**, 180 (1997); Phys. Rev. Lett. **79**, 26 (1997).

[127] D. Adams *et al.* (Spin Muon Collaboration), Phys. Lett. B **357**, 248 (1995).

[128] S. E. Kuhn, J.-P. Chen, and E. Leader, arXiv:0812.3535.

[129] B. Julia-Diaz, D. O. Riska, and F. Coester, Phys. Rev. C **69**, 035212 (2004); **75**, 069902 (2007).

[130] S. Wandzura and F. Wilczek, Phys. Lett. **72B**, 195 (1977).

[131] E. V. Shuryak and A. I. Vainshtein, Nucl. Phys. **B201**, 141 (1982).

[132] For a review on $g_2^a(x) \equiv g_T^a(x) - g_1^a(x)$ see R. L. Jaffe, Comments Nucl. Part. Phys. **19**, 239 (1990).

[133] X. Zheng *et al.* (Jefferson Lab Hall A Collaboration), Phys. Rev. C **70**, 065207 (2004).

[134] M. Amarian *et al.* (Jefferson Lab E94-010 Collaboration), Phys. Rev. Lett. **92**, 022301 (2004).

[135] P. L. Anthony *et al.* (E155 Collaboration), Phys. Lett. B **553**, 18 (2003).

[136] M. Hirai, S. Kumano, and M. Miyama, Comput. Phys. Commun. **111**, 150 (1998).

[137] B. Pasquini, S. Boffi, A. V. Efremov, and P. Schweitzer, arXiv:0903.1830-hep-ph.

[138] P. Schweitzer, D. Urbano, M. V. Polyakov, C. Weiss, P. V. Pobylitsa, and K. Goeke, Phys. Rev. D **64**, 034013 (2001); K. Goeke *et al.*, Acta Phys. Pol. B **32**, 1201 (2001).

[139] H. Avakian *et al.*, JLab Report No. E05-113.

[140] H. Avakian *et al.*, JLab Report No. PR12-07-107.

[141] H. Avakian, *et al.*, JLab Report No. LOI 12-06-108, 2008.

[142] B. Adeva *et al.* (Spin Muon Collaboration), Phys. Lett. B **420**, 180 (1998).

[143] A. Airapetian *et al.* (HERMES Collaboration), Phys. Rev. D **71**, 012003 (2005).